T.C.
ISTANBUL OKAN UNIVERSITY
INSTITUTE OF GRADUATE SCIENCES

THESIS

FOR THE DEGREE OF

MASTER OF SCIENCE

IN ADVANCED ELECTRONICS AND

COMMUNICATION TECHNOLOGIES PROGRAM

Hayder Sami Abbas AL GBURI

INVESTIGATION OF VISIBLE LIGHT COMMUNICATION CHANNEL PERFORMANCE UNDER DIFFERENT NOISE LEVEL CONDITIONS

ADVISOR

Dr. Öğr. Üyesi Didem KIVANÇ TÜRELİ

ISTANBUL, July 2023

T.C.
ISTANBUL OKAN UNIVERSITY
INSTITUTE OF GRADUATE SCIENCES

THESIS

FOR THE DEGREE OF

MASTER OF SCIENCE

IN ADVANCED ELECTRONICS AND

COMMUNICATION TECHNOLOGIES PROGRAM

Hayder Sami Abbas AL GBURI
(203006001)

INVESTIGATION OF VISIBLE LIGHT COMMUNICATION CHANNEL PERFORMANCE UNDER DIFFERENT NOISE LEVEL CONDITIONS

ADVISOR
Dr. Öğr. Üyesi Didem KIVANÇ TÜRELİ

ISTANBUL, July 2023

T.C.

ISTANBUL OKAN UNIVERSITY
INSTITUTE OF GRADUATE SCIENCES

THESIS FOR THE DEGREE OF MASTER OF SCIENCE
IN ADVANCED ELECTRONICS AND
COMMUNICATION TECHNOLOGIES PROGRAM

Hayder Sami Abbas AL GBURI
(203006001)

INVESTIGATION OF VISIBLE LIGHT COMMUNICATION CHANNEL PERFORMANCE UNDER DIFFERENT NOISE LEVEL CONDITIONS

Date Thesis Delivered to Institute : June 20, 2023
Date of Thesis Defense : July 20, 2023

Thesis Advisor: Dr. Öğr. Üy. Didem KIVANÇ TÜRELİ _____
Thesis Co-Advisor: Prof. Dr.Ahmed Abd Al-kareem ALI _____
Jury Members: Dr. Öğr. Üy. Sina MOJTAHEDI _____
Doç. Dr. Ömer Cihan KIVANÇ _____
Prof. Dr. Mehmet Serdar Ufuk TÜRELİ _____

ISTANBUL, July 2023

ABSTRACT

INVESTIGATION OF VISIBLE LIGHT COMMUNICATION CHANNEL PERFORMANCE UNDER DIFFERENT NOISE LEVEL CONDITIONS

The performance communication systems across wireless channels is limited by fading. A proposed method for fast wireless communication is visible light communication (VLC). However, a number of variables, including channel conditions, bit rate, and outside noise, can have an impact on how well VLC systems perform. This thesis presents a study of the performance of VLC systems under various operation conditions. The work was carried out using Optisystem and MATLAB software for channel modeling. Performance was tested based on bit error rate (BER) and eye diagram.

The study's findings demonstrated that as bit rate and outside noise increase, so does the BER of VLC systems. Along with increased external noise and bit rate, the eye diagram closes and the probability of bit error increases. Adaptive modulation and coding techniques can boost the performance of VLC systems. These methods enable dynamic modulation scheme and coding rate adaptation to the current channel conditions. The results of this study can be used to design and optimize VLC systems for different applications.

Keywords: Visible Light Communication, OptiSystem, Matlab.

KISA ÖZET

GÖRÜNÜR IŞIK İLETİŞİM SİSTEMİNİN FARKLI GÜRÜLTÜ SEVİYESİ KOŞULLARI ALTINDA İNCELENMESİ

Kablosuz iletişim sistemlerinin performansı sönümleme ile sınırlıdır. Hızlı kablosuz iletişim için önerilen bir yöntem, görünür ışık iletişimidir (VLC). Ancak kanal koşulları, bit hızı ve dış gürültü dahil olmak üzere bir dizi değişken, VLC sistemlerinin performansını etkileyebilir. Bu tez, çeşitli çalışma koşulları altında VLC sistemlerinin performansına ilişkin bir çalışma sunmaktadır. Çalışma, kanal modelleme için Optisystem ve MATLAB yazılımı kullanılarak gerçekleştirilmiştir. Sistem performansı, bit hata oranı (BER) ve göz diyagramı temel alınarak test edildir.

Çalışmanın bulguları, bit hızı ve dış gürültü arttıkça VLC sistemlerinin BER'inin de arttığını gösterdi. Gürültü ve bit hızının artmasıyla birlikte göz diyagramı kapanır ve bit hata oranı yükselir. Uyarlanabilir modülasyon ve kodlama teknikleri VLC sistemlerinin performansını artırabilir. Bu yöntemler, dinamik modülasyon şemasını ve mevcut kanal koşullarına kodlama hızı adaptasyonunu mümkün kılar. Bu çalışmanın sonuçları, farklı uygulamalar için VLC sistemlerini tasarlamak ve optimize etmek için kullanılabilir.

Anahtar Sözcükler: Görünür Işık İletişimi, araç iletişimi, OptiSystem, Matlab.

To My Family

ACKNOWLEDGMENT

Thank you to my family for their support during my thesis.

TABLE OF CONTENTS

I. INTRODUCTION 1

1.1. INTRODUCTION 1
1.2. OBJECTIVES 2
1.3. LITERATURE SURVEY 2
1.4. STRUCTURE OF THESIS 12

II. BASIC PRINCIPLES OF VISIBLE LIGHT COMMUNICATIONS TECHNOLOGY 13

2.1. INTRODUCTION 13
2.2. BASIS OF VLC TECHNOLOGY 13
2.3. DATA TRANSFER AND RECEPTION IN VLC TECHNOLOGY 14
2.4. VLC COMMUNICATION MEDIUM AND NOISE INTERFERENCE 15
2.5. CHANNEL EFFECTS 20
2.6. VLC SYSTEM COMPONENTS 22
2.6.1. LED 22
2.6.2. LED Construction 25
2.6.3. Channel Impairments 27
2.6.4. Optical Detectors 30
2.6.5. Filters 33
2.7. NOISE TYPES IN PIN PHOTODETECTORS 37
2.7.1. Shot Noise 37
2.7.2. Thermal Noise 38
2.7.3. Dark Current Noise 39
2.7.4. Quantum Noise 40
2.7.5. 1/f Noise 41
2.8. PERFORMANCE CHARACTERISTICS 41
2.8.1. Responsivity 41
2.8.2. Bandwidth 42

III. SYSTEM MODELING AND RESULTS 43

3.1. INTRODUCTION 43
3.2. VLC SYSTEM SIMULATION 43
3.3. VLC CHANNEL 46
3.4. OPTISYSTEM ANALYSIS TOOLS 49
3.4.1. Eye Diagram and Q Factor 49
3.4.2. BER Analyzer 52
3.5. SYSTEM PARAMETERS 52
3.6. RESULTS 60

IV. SUMMARY AND CONCLUSIONS 67

LIST OF TABLES

Table III.1. Main component configuration..... 46

LIST OF FIGURES

Figure II.1. System Model. 14

Figure II.2. VLC channel and FoV. 17

Figure II.3. Angles of incidence and irradiance. 17

Figure II.4. Polar and azimuth angles [35]. 20

Figure II.5. A duplex VLC transmission system [16]. 22

Figure II.6. Recombination across PN junction. 23

Figure II.7. LED structure. 26

Figure II.8. Turbulent channel at a fixed time. 30

Figure II.9. Avalanche photodiodes structure and operation 33

Figure II.10. Frequency response of LP filter. 35

Figure II.11. Frequency response of HP filter. 36

Figure II.12. Frequency response of BP filter. 37

Figure III.1. OptiSystem model. 44

Figure III.2. Matlab model flowchart. 47

Figure III.3. OptiSystem model flowchart. 48

Figure III.4. Eye diagram [63]. 50

Figure III.5. Random bits. 53

Figure III.6. NRZ symbols. 53

Figure III.7. LED source frequency response. 54

Figure III.8. LED source time response. 55

Figure III.9. Power meter for LED. 55

Figure III.10. White light source power reading (a) 3 W (b) 0.2 W (c) 1 W. 56

Figure III.11. Frequency response of the white light source. 57

Figure III.12. Time response for 10 bits with 0.5W. 58

Figure III.13. Time response for 10 bits with 1W. 58

Figure III.14. Time response for 10 bits with 2W. 59

Figure III.15. Compare the original bits from PRBS generator (red signal) with signal after lowpass rectangular filter (blue signal). 60

Figure III.16. Eye diagrams of received signal at 1 meter distance. 61

Figure III.17. Q factor values with distance at different external noise at data rate 0.8Gbps. 62

Figure III.18. Q factor values with distance at different external noise at data rate 0.9Gbps. 63

Figure III.19. Q factor values with distance at different external noise at data rate 1Gbps. 63

Figure III.20. Q factor values with distance at different external noise at data rate 1.2Gbps. 63

Figure III.21. Q factor values with distance at different external noise at data rate 1.5Gbps. 64

Figure III.22. BER across distance at different external noise at data rate 0.8 Gbps. 65

Figure III.23. BER across distance at different external noise at data rate 0.9 Gbps. 65

Figure III.24. BER across distance at different external noise at data rate 1 Gbps. 65

Figure III.25. BER across distance at different external noise at data rate 1.2 Gbps. 66

Figure III.26. BER across distance at different external noise at data rate 1.5 Gbps. 66

SYMBOLS

h	Planck's constant. ($h \approx 6.626 \times 10^{-34}$ Joule-seconds)
k	Boltzmann's constant. ($k \approx 1.38064852 \times 10^{-23}$ Joules per Kelvin),
$\boldsymbol{\theta}$	polar angle.
$\boldsymbol{\omega}$	azimuth angle of device.
$\boldsymbol{\psi}$	angle of incidence to device.
A_{geo}	geometrical loss.
A_{atm}	atmospheric attenuation.
A_{fog}	attenuation due to fog.
A_{rain}	attenuation due to rain.
λ	photon wavelength.
T	temperature.
B	bandwidth.

ABBREVIATIONS

ADC Analog-to-digital converter

FOV Field of View

LED Light Emitting Diode

PD Photodetector

RF Radio Frequency

TIA Transimpedance Amplifier

VLC Visible Light Communication

V2LC Vehicular Visible Light Communication

V-VLC Vehicular Visible Light Communication

VNA Vector Network Analyzer

EUB Effective Usable Bandwidth

LD Laser Diode

IM Intensity Modulation

COTS Commercial Off The Shelf

AF Amplify and Forward

AT Atmospheric Turbulance

I. INTRODUCTION

1.1. Introduction

Visible Light Communication (VLC) is a wireless communication technology that uses the visible light spectrum (380-780 nm) to transmit data. VLC has attracted attention recently due to its high capacity, localized security, and ability to operate in unlicensed spectrum. The visible light spectrum has a much larger bandwidth than the radio frequency (RF) spectrum, which allows for much higher data rates in VLC systems. For example, VLC systems can achieve data rates of up to 10 Gbps, while RF systems are typically limited to a few Mbps.

VLC signals are also more secure than RF signals because they are directional. This means that only receivers that are in the direct path of the light beam can receive the signal. This makes it difficult for unauthorized users to intercept VLC signals. In addition, VLC signals cannot travel through walls, which makes them ideal for use in RF-sensitive environments such as hospitals and airplanes. Finally, VLC can be used to provide both illumination and communication simultaneously. This is more efficient than using separate systems for each, as it reduces the amount of energy that is wasted.

The roots of VLC date back to the semaphore systems used in the last century, and technology has received continuous interest since then [1][2]. Alexander Graham Bell, who invented the telephone, also demonstrated a “photophone” in 1880. The term VLC was introduced in 2003 at Nakagawa Laboratory in Keio University, Japan, where studies were conducted on the use of light-emitting diodes (LEDs) for VLC [3]. Since then, there has been a growing interest in VLC research and development. This is due in part to the advances that have been made in LED technology. LEDs are now

much brighter, more efficient, and easier to control than they were in the past. This makes them ideal for use in VLC systems.

This work studies the performance of a VLC system under different operating conditions. OptiSystem software from Optiwave [4] were used to simulate system components, while MATLAB were used to simulate the wireless channel and fading parameters

1.2. Objectives

The following are the goals of this study:

1. Investigate the effect of VLC channel length on the system performance (Bit Error Rate and quality factor.
2. Investigate the effect of external noise (sun light and other lightening) on the VLC system performance.
3. Introduce the MATLAB channel modeling to OptiSystem to overcome the limitations of wireless channel model available in software
4. Investigate the maximum transmutation bit rate achieved with allowable BER.

1.3. Literature survey

VLC systems are very attractive for their capabilities, particularly for vehicular communications [5]. They are of interest particularly for 6G communications [6] in vehicular networks [7]. Following is a survey of relevant recent research related to VLC systems.

A. R. Ndjiongue and H. C. Ferreira (2018) [8] present an overview of outdoor applications of visible light communications (VLC) technology, which has received

less attention than indoor ones. The drawbacks of outdoor VLC include difficulties with LED use, increased interference and noise levels, and the existence of substitute communication technologies that are more suited for outside settings. Numerous outdoor VLC applications, including building-to-building (B2B), vehicle-to-vehicle (V2V), road-to-vehicle (R2V), and the deployment of Li-Fi using street and park lighting, have been identified despite these difficulties. Even better, some solutions make use of solar panels' dual functionality as VLC antennas and electrical energy harvesters. The implementation of outdoor VLC systems presents a number of obstacles, including those related to geometric elements of light diffusion and environmental variables like fog, rain, sunlight, and air disturbances. The outdoor VLC environment offers a wide range of study prospects despite its difficulties. The article examines promising applications, groups them into categories, and recommends likely research prospects in the area of telecommunication engineering. Overall, this survey stimulates more investigation and study in this field while offering insightful information about the possibilities of outdoor VLC.

A. Memedi and F. Dressler (2021) [5] present a survey on vehicular visible light communication (VVLC). They list many applications including information retrieval about road conditions and intersections, and cooperative driving applications such as platooning. They present an overview of possible sources for the optical signal such as headlights and tail lights and their properties and receivers. They also present properties of VVLC channels and the environmental factors which affect these channels.

E. Zadobrischi and M. Dimian (2021) [9] present some scenarios in which vehicular communication can be used to reduce accidents. Protocols was developed

describing the behavior of the vehicles in the event of receiving a warning message from another vehicle or from a road side unit. Simulations were used to find the latency and rate of successful packet reception as a function of the number of hops between vehicles before successful packet delivery.

B. Turan, G. Gurbilek *et. al.* [10][11][12] have conducted both experimental [10][11] and simulation [12] studies on vehicular visible light communication (V2LC). In initial studies B. Turan *et. al.* (2018) [10] study uses a vector network analyzer (VNA) as a transmitter and receiver, driving COTS automotive light emitting diodes (LEDs) to emit light and an avalanche diode for detection. They examine outdoor V2LC channel characteristics under different illumination conditions (night, sunset, and sunlight). The authors present the idea of effective useable bandwidth (EUB) as a useful criterion for evaluating the performance of V2LC systems based on actual measurements. The findings show that inter-vehicular communication can efficiently make use of the 30 dB modulation bandwidths of LEDs, with the benefit of increased optical power at higher modulation frequencies. However, because photo-detectors (PDs) have a limited dynamic range, it is discovered that the EUB is affected by the surrounding lighting and inter-vehicle distances. The root mean square (RMS) delay spread varies at distances higher than 6 m due to the availability of range-finding sensors and ambient light sensors in current vehicles, with road reflections becoming more noticeable as inter-vehicular distance rises. The study shows the importance of LED design in defining the V2LC channel and the opportunities and challenges that could arise when putting V2LC systems into practice. In further experimental studies

Gurbilek *et. al.* (2019) [11], improved their experimental setup by adding software defined radio (SDR) units to the receiver. With this setup they are able to

implement OFDM modulation. This work studies the frequency response of various models of COTS LED headlights and compares their frequency response using a vector network analyzer (VNA). Further, using these headlights as transmitters and an avalanche photodetector and SDR as a receiver and several OFDM based modulation schemes. They find that the nonlinear response of the transmitters and clipping must be taken into account in comparing modulation schemes.

Using the data from these experiments, Gurbilek *et. al.* (2023) [12] find that the normalized channel response does not depend on the relative positions of the transmitter and receiver or of ambient light. They then derive an algorithm for blind channel estimation for ODFM based VVLC systems.

Turan and Coleri (2021) [13] use a more elaborate experimental system involving Lidar, GPS and other input data to develop a machine learning model to predict channel conditions. The inputs to the model include the type of LED transmitter and PD receiver, the input from a light sensor measuring ambient sunlight, the engine speed of the front vehicle (which effects exhaust gasses, potentially interrupting the VLC link), road surface and environment data, and most importantly the relative positions of vehicles in the environment. The system outputs are the path loss and frequency response of the channel. The convergence and accuracy of the models are compared.

Amjad *et. al.* (2021) [14] present results from another vehicular VLC testbed. Their testbed uses the open source GNURadio software on the USRP software defined radios, with an LED headlight for transmission. For VLC reception, the system uses a photodetector with biconvex lenses used to focus more light on the photodetector,

which also has a Transimpedance Amplifier (TIA). They realize OFDM based communications which is compliant with IEEE 802.11 type systems.

A. R. Ndjiongue *et. al.* (2020) [15] examine the possibilities of visible light communication (VLC) for outdoor positioning. While numerous indoor VLC-based locating systems have been developed, there is a dearth of studies on visible light outside placement. The problems and disadvantages of employing visible light for outdoor positioning are discussed in the first section of the paper. The assessment of current visible light-based indoor location systems is followed by an analysis of the difficulties in applying them to outdoor placement. The study emphasizes how crucial it is to handle ambient light conditions because they have a substantial impact on the efficiency and dependability of VLC-based locating systems, especially in outdoor settings. Overall, this study illuminates the state of outdoor location using visible light today and offers perceptions into the advantages and disadvantages that researchers and developers should take into account while pursuing this technology for outdoor applications.

Aboagye, Ndjiongue *et. al.* (2023) [16][17] also present a tutorial on the use of reflective intelligent surfaces (RIS) on VLC systems. Since VLC is highly directive and reflective, the angle between the PD surface and the arriving of the field of view (FoV) is critically important for these applications. VLC receivers commonly contain a lens placed in front of the PD to refract light and focus maximum energy onto the PD. In the dynamic environment of VLC it may be advantageous to replace this lens with a smart lens, with an adjustable material or shape. The authors give two examples of such lenses, the LCD lens and the meta-lens and discuss their advantages and disadvantages compared to traditional focusing lenses.

R. C. Fon *et. al.* (2019) [18] discuss how Visible Light Communications (VLC) technology's constrained transmission range has impeded its use as an access system technology. The primary reason for VLC's narrow range is its constrained lighting range, which limits its use to specific situations involving nearby communication nodes both inside and outside. In order to get over this restriction, the study suggests using a fiber optic (FO) communication system and switching to LED driven VLC for indoor communication. To cut down on deployment expenses and the latency introduced by transducing from light to electric signals and re-encoding for the indoor system, the system incorporates an amplify-and-forward (AF) technique. The entire channel frequency response is shown in the study while taking into account a number of transmitting factors, including the indoor reflection coefficient, outdoor transmission distance, and fiber optic attenuation coefficient.

R. C. Fon *et. al.* (2023) [19] further extends this study to compare to a second cascaded VLC system. In this second system, the outdoor link is also a free space ink but uses a laser diode (LD) across free space. The study analyses the proposed systems' channel performance and discusses how various transmission environment characteristics affect data transfer. Both methods allow all-optical high bandwidth low latency communication across longer distances compared to stand alone LED VLC links. The potential advantages and difficulties of putting such a cascaded VLC system into place are examined.

Al-Kinani *et. al.* (2018) [20] give a survey of VLC channel modeling, introducing the different scenarios for optical communication and channel characteristics which must be taken into account. They give an overview of indoor, outdoor and underwater

VLC systems, however since until 2018 most work was on indoor VLC, the work largely focuses on indoor VLC.

Alsalami *et. al.* (2019) [21] proposes a channel model for V2LC systems. They study a geometrical approach and analyze the effect of the location and velocity of the vehicle as well as the effect of reflections. The transmitting vehicle, the receiving vehicle and the vehicle generating a reflection of the signal form an ellipse, which is used to calculate the channel. By studying random position for the reflecting vehicle, a stochastic geometrical channel model is defined.

Alsalami *et. al.* (2022) [22] further extend their work to study the impact of traffic surrounding the V2V link on channel conditions. They also analyze the effect of using low and high beam headlights on the link. The simulations are based on real hourly traffic data collected from the UK. The error rate is calculated for various times of day and night and low and high beam headlight use. They find that it is possible to connect the link using non line of sight propagation during rush hour, while at night in low traffic direct line of sight communication is possible. High beam headlights give more light, ensuring a lower error rate under the same conditions.

R. W. Zaki *et. al.* (2019) [23] investigate outdoor visible light communication (VLC) in various weather scenarios, with a particular emphasis on the effects of snow and rain attenuation on the effectiveness of the VLC system. Using the Marshal, Carbonneau, and Japan models for rain attenuation and the wet and dry snow conditions for snow attenuation, respectively, the research analyses various precipitation amounts. In the context of outdoor VLC design characteristics like signal-to-noise ratio (SNR), optical power received, bit error rate (BER), and maximum coverage area, a number of modulation techniques, including ON-OFF Keying (OOK),

L-Pulse Position Modulation (L-PPM), Inverse L-Pulse Position Modulation (I-L-PPM), and Subcarrier Binary Phase-Shift Keying (SC-BPSK), are investigated. Based on the type of modulation technique utilized, simulation findings demonstrate the significant variations in information received under various weather situations. A green LED, which served as the transmitter, and a non-imaging concentrator connected to a photodetector, which served as the receiver at a reasonable price are all described in the study. The study's analysis of the effects of weather-related attenuation on VLC performance finishes by naming L-PPM as the modulation method most likely to achieve greater coverage distances. The literature review demonstrates the potential of VLC technology in intelligent transport systems (ITS) and highlights its sensitivity to weather conditions. It also offers useful insights into the opportunities and constraints connected with outdoor VLC systems. Researchers and engineers looking to create reliable outdoor VLC communication systems might benefit from the in-depth investigation and comparison of various modulation schemes.

Avatamanitei *et. al.* (2020) [24][25] examine how snowfall affects outdoor visible light communications (VLC) and its possible effects on data transmission between moving vehicles and between moving vehicles and traffic infrastructure. The research emphasizes the significance of dependable wireless communication technologies in raising the security and effectiveness of road transport. This study focuses on VLC as a viable remedy for present wireless technologies that have reliability difficulties in automobile applications. The experiment involved testing a 50-meter VLC link in a variety of snowfall scenarios, from mild snowfall to heavy snowfall and storm occurrences. According to the research, light snowfall has much less impact on VLC performance, but heavy snowfall and blizzards have a

considerable impact on the Bit Error Ratio (BER). Overall, the research illustrates VLC's potential to continue to offer data connectivity even under adverse weather circumstances while also providing experimental proof of the disruptive impacts of snowfall, particularly with wind, on outdoor VLC. The results indicate that VLC has potential as a wireless communication technology for automotive applications, and VLC communication is still achievable even in a snowstorm, especially with performance gains through error-correction methods under more severe weather scenarios.

Avatamanitei *et. al.* (2021) [26] continue with further experiments, improving their experimental setup with new amplifiers and lenses. The transmitter and receiver are an LED traffic light and a PIN photodiode. Through testing VVLC at distances of 75 meters [26] and 188 meters [27], the authors have noted that communication is still relatively robust even at these distances.

H. Eldeeb *et. al.* (2021) [28] adopt a semi-analytical approach to find a closed-loop solution for the average BER on an infrastructure to vehicle VLC channel. They use commercial ray tracing software to simulate a two lane highway scenario with the transmitter located at a streetlight on the road. They then use the channel impulse responses derived from the simulation to calculate fundamental statistical properties of the channel such as the length of the impulse response and the magnitude and spacing of multipath components. It is also found that the average received signal power tends to increase and decrease following a sinusoidal pattern with distance from the source. For the scenario it is found that a two path channel accurately models the received signal power, and a statistical model is developed for the relative power of the second path. These factors are input to the analytical formulas for M-ary Pulse

Amplitude Modulation (PAM) which is the modulation scheme for this scenario, leading to a closed form solution for the BER terms of the pole height, vehicle height, pole spacing and distance of the vehicle from the side of the road.

E. Eso, *et. al.* (2021) [29] study the effect of atmospheric turbulence (AT) on VVLC. AT occurs when there are gasses of very different temperature next to each other, distorting the received light signal. This may be due to the heat on the road on a hot day or due to exhaust gasses from the tailpipes of vehicles. This paper performs analytical, simulation and experimental studies of AT. Their work shows that aperture averaging can effectively cancel out the effect of AT.

M. Huang, *et. al.* (2018) [30] focuses on a slightly different problem, that of locating the transmitting LEDs. They presente an enhanced particle filter technique and the Continuously Adaptive Mean Shift (Cam-Shift) method for outdoor-VLC. The camshaft algorithm is well known in computer vision. It uses color to identify the object being tracked. By finding histograms of the color distribution of a block of pixels in the image, it tracks the image from frame to frame. The Light Emitting Diode (LED) area in the outdoor-VLC system is the target signal source that this article is focused on precisely and thoroughly tracking. The study focuses on the problems brought on by numerous environmental interferences, such as background interference and comparable object interference, which can make the tracking and extraction process more difficult. The proposed algorithm provides precise, stable, and real-time tracking and extraction of the target LED region under various environmental interferences, with the goal of increasing the viability of practical implementations of VLC systems in outdoor scenarios. Even in the face of several interference elements, experimental findings show the algorithm's usefulness in terms of accuracy, resilience,

and real-time performance. By tackling the crucial issue of tracking and extracting the target signal source LED area, the proposed algorithm closes the gap in the existing VLC research and establishes a basis for effective VLC communication in dynamic outdoor contexts. Overall, this paper demonstrates the importance of the suggested algorithm in enhancing the viability and usability of outdoor-VLC applications, and it advances the development of image-sensor-based VLC systems for both indoor and outdoor environments.

1.4. Structure of Thesis

Five chapters make up this thesis. Chapter 1 covers introduction and literature survey. Theoretical background of the VLC system and its components will be covered in chapter two. Chapter three illustrate the VLC system simulation and present the main obtained results that will be discussed in chapter four. The conclusion and suggestions for further research are covered in Chapter 5.

II. BASIC PRINCIPLES OF VISIBLE LIGHT COMMUNICATIONS TECHNOLOGY

2.1. Introduction

This chapter thoroughly explored the essential components that support Visible Light Communications (VLC) technology, along with data transmission and detection methods, the communication channel and sources of interference and noise, and practical mitigation techniques, performance improvement strategies.

2.2. Basis of VLC Technology

Similar to a number of Optical Wireless Communications (OWC) technologies, VLC technology takes advantage of LEDs' quick switching speed to incorporate data into the light output, shown in Figure III.1. The data modifies the light intensity, in general this flicker is fast and not high amplitude so that it is not observable to the human eye. The communication signal is carried by this light as it travels towards the Photodetector (PD). At the receiving end, the PD and transconductance amplifier (TIA) read the light intensity to generate a voltage signal that the signal processing module can process [31][32].

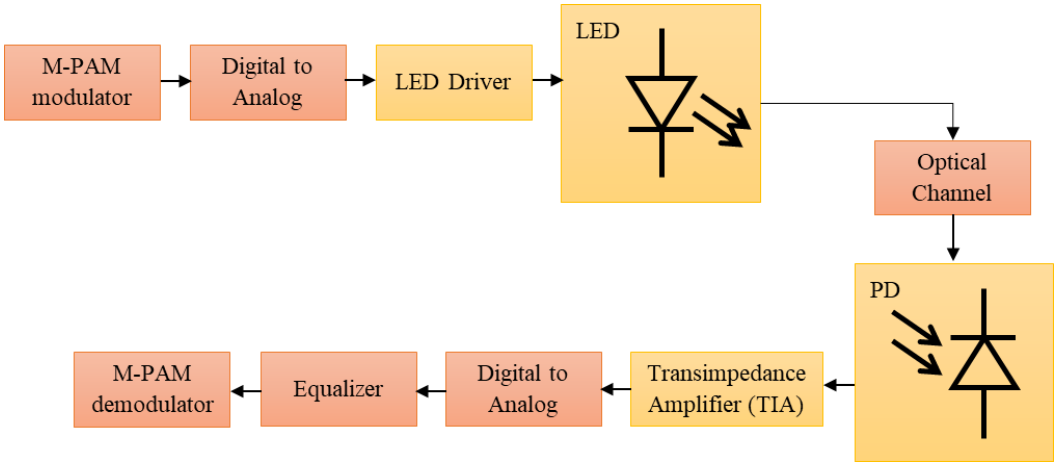

Figure II.1. System Model.

The limited modulation bandwidth that arises from LEDs entering saturation state as the modulation frequency increases is a significant drawback of VLC technology. Additionally, a real and positive signal must be transmitted.

2.3. Data Transfer and Reception in VLC Technology

VLC Signal Transfer: A thorough examination of the transmitter in Figure II.1 reveals that a VLC transmitter's architecture differs from traditional versions in terms of the composition of its component blocks. For instance, an LED driver, a crucial component of VLC, is not necessary for an RF transmitter. The VLC encoder plays a similar purpose as the RF variant. Nevertheless, because VLC signals are only positive and genuine, the modulator may be different from those used in RF. In Section III-D, we go into the procedure related to asymmetrically conveyed VLC signals.

Laser Diode (LD) and LED are the two primary diode types used in VLC technology's light source package. Both employ intensity modulation (IM), a method that modifies the current intensity flowing through the LD/LED in response to

incoming bits, often transmitting the modified intensity's waveform to the next light beam.

There are numerous kinds of luminescent diodes, categorized by the wavelength or the way that light is made. These include organic LEDs, Quantum dot LEDs, high-power LEDs, red-green-blue LEDs, IR-LEDs, ultraviolet-LEDs, LDs, and phosphor-LEDs. Light-emitting semiconductors were first created in a variety of colors (or non-visible colors) and wavelengths, such as yellow for wavelengths between 570 and 590 nm, red for wavelengths between 610 and 760 nm, blue for wavelengths between 450 and 500 nm, and green for wavelengths between 500 and 570 nm. The range for LDs is 630 nm to 950 nm.

VLC Signal Reception: Direct detection (DD) or heterodyne modes may be used at the receiving end for detection. However, there are advantages in terms of cost and complexity from IM/DD integration. The PD and TIA are particular parts of VLC detectors that set the VLC receiver apart from the RF receiver.

The doping structure of PDs is often similar to that of light-emitting semiconductors. A PD must be innately tuned to detect the appropriate frequency range, meaning sensitivity to that particular wavelength, in order to recognize a given waveform. As a result, a laser PD responds to a signal from an LD, an IR-PD absorbs light from an IR-LED, and so on. The receiver as a whole is a cost-effective equipment since PDs, like LEDs and LDs, are inexpensive and low-power components.

2.4. VLC Communication Medium and Noise Interference

The transmitting and receiving antennas are linked by the VLC medium, which in this case is the light source and the PD. This communication medium functions

similarly to all other communications technologies. The optical component of the VLC system is represented by this medium.

Optical path loss and multi-path induced dispersion are experienced by the VLC medium. The extent to which the medium affects the broadcast signal, however, is typically determined by the configuration of the VLC system. Since reflections from light components are not taken into account for Line of Sight (LoS) configurations, the VLC medium primarily experiences path loss, which can be easily computed from the knowledge of the transmitter beam divergence, receiver size, and separation distance.

The VLC medium is characterized by its sensitivity to shadowing and obstacles as well as the effect of the device's orientation. Because VLC signals have a short wavelength, when they encounter opaque barriers, such as the human body, they cast distinctive shadows. A receiver in the darkened area experiences communication interruption as a result.

The core idea of a simple VLC system is shown in Figure II.2, which also emphasizes the dual function of the light source in providing both illumination and data. The geometrical relationship between the source of light, the receiver are shown in the figure. The receiver's Field of View (FoV) is a very important parameter, the light source must fall into the FoV for correct reception of the signal.

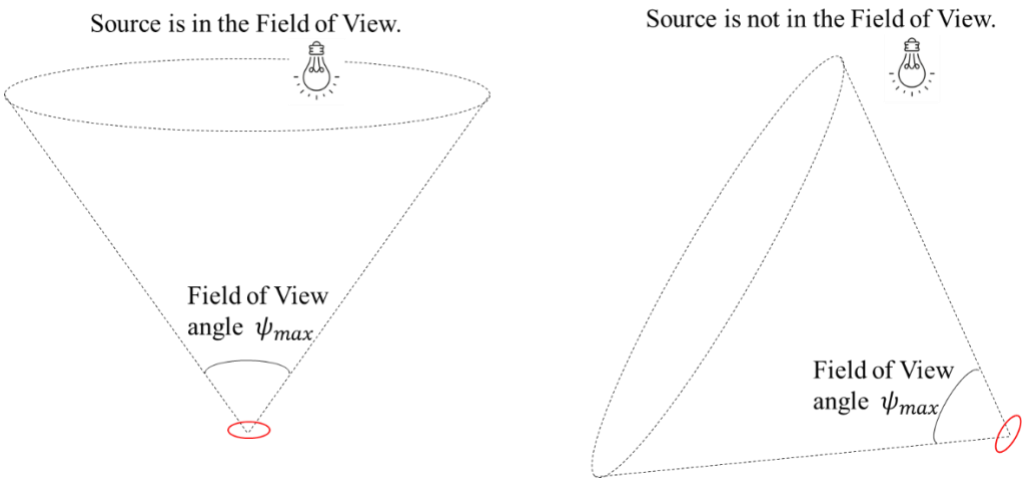

Figure II.2. VLC channel and FoV.

The light intensity for an LED is modeled to have a Lambertian distribution [33]. Figure II.2 represents Field of View and how it changes when the receiving PD is angled away from the source. Figure II.3 illustrates the incidence and irradiance angles for the link. The distance between the light source and the PD, the receiver's field of view, the receiving angle, and the PD's sensitivity are all included in the overall channel gain.

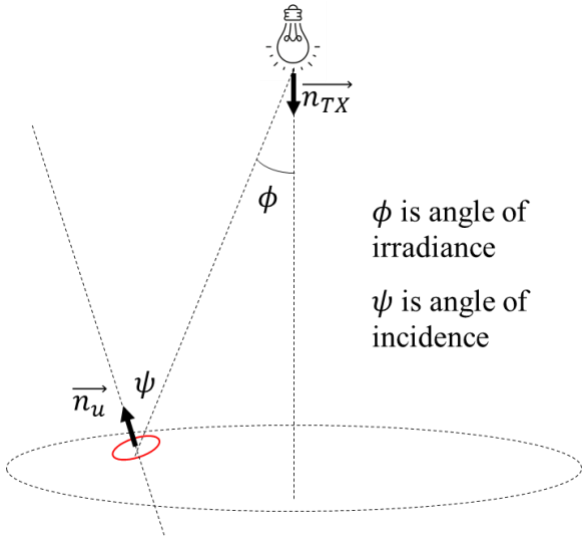

Figure II.3. Angles of incidence and irradiance.

The power of the light signal received is

$$P_r = I_s(d, \phi)\, A_{eff}(\psi) \tag{II.1}$$

where $I_s(d, \phi)$ is the irradiance on the PD and $A_{eff}(\psi)$ is the effective area of the PD, including filtering and lenses.

The effective area of the PD will depend on the physical area of the PD, as well as the effect of the concentrator and filter that are used with it:

$$A_{eff}(\psi) = \mathrm{A}\, T_s(\psi)\, g(\psi) \cos(\psi) \tag{II.2}$$

$T_s(\psi)$ is the effect of the filter, which can depend on light wavelength as well as angle of incidence. $g(\psi)$ is the concentrator gain, given by:

$$g(\psi) = \left(\frac{n}{\sin(\psi_{max})}\right) \tag{II.3}$$

where n is the refractive index of the medium (1 for air).

The irradiance depends on the transmit power P_t and the radiant intensity R_0

$$I_s(d, \phi) = P_t R_0(\phi) \tag{II.4}$$

The Lambertian radiant intensity is often used:

$$R_0(\phi) = \frac{(m+1)}{2\pi} \cos^m(\phi) \tag{II.5}$$

The parameter m is

$$m = \frac{-\ln(2)}{\ln\left(\cos \phi_{1/2}\right)} \tag{II.6}$$

where $\phi_{1/2}$ is a property of the transmitter, giving the angle at which the transmitted power drops to half the power at the center of the beam when the device is transmitting at half power.

However this thesis considers a Gaussian beamforming shape, where the incidence on the PD is calculated from the divergence angle of the source θ_{div} as:

$$w_0 = w_0(\lambda, \theta_{div}) = \frac{\lambda}{\pi\, \theta_{div}} \tag{II.7}$$

$$z_R = \frac{\pi\, {w_0}^2}{\lambda} = \frac{\pi}{\lambda} \times \frac{\lambda^2}{\pi^2\, {\theta_{div}}^2} = \frac{\lambda}{\pi\, {\theta_{div}}^2} \tag{II.8}$$

$$w(z) = w_0 \sqrt{1 + \left(\frac{z}{z_R}\right)^2} \tag{II.9}$$

$$I_s(z) = P_t \frac{1}{\pi\, (w(z))^2} \tag{II.10}$$

Here, $w(z)$ is the beam radius, or how far away the PD must be from the center of the beam axis for the beam power to drop to $1/e^2$ of the maximum value [34] and z_R is the Rayleigh length.

Finally the gain of the channel, whenever the transmitter is within the FoV for the receiver, is given by:

$$\begin{aligned} H(0)_{LOS} &= \frac{A_0}{d^2} R_0(\phi) T_s(\psi) g(\psi) \cos(\psi) \\ &= \frac{(m+1)A_0}{2\pi d^2} \cos^m(\phi)\, T_s(\psi) g(\psi) \cos(\psi) \end{aligned} \tag{II.11}$$

When the transmitter is not within the FoV, no signal can be received so the gain is 0. The above derivation is assuming Lambertian model and line of sight (LOS) signal reception with no multipath components. Non line of sight (NLOS) signal components are not considered in this thesis.

Fields of View (FoV) on PDs are constrained, since sensors receive much higher power when the signal arrives orthogonal to the PD. If the device orientation changes so it faces further away from the source of the signal, the signal may not be picked up at all. The maximum angle at which a signal is received is called the Field of View angle. The user's device's random orientation has no effect on the angle of irradiance,

but has a significant impact on the angle of incidence. The polar angle $\boldsymbol{\theta}$ and azimuth angle $\boldsymbol{\omega}$ of the instrument can be used to represent the cosine of the angle of incidence $\boldsymbol{\psi}$, as shown in [35], as follows:

$$\cos(\psi) = (x_a/d)\sin(\theta)\cos(\omega) + (y_a/d)\sin(\theta)\cos(\omega) + (z_a/d)\sin(\theta) \quad \text{(II.12)}$$

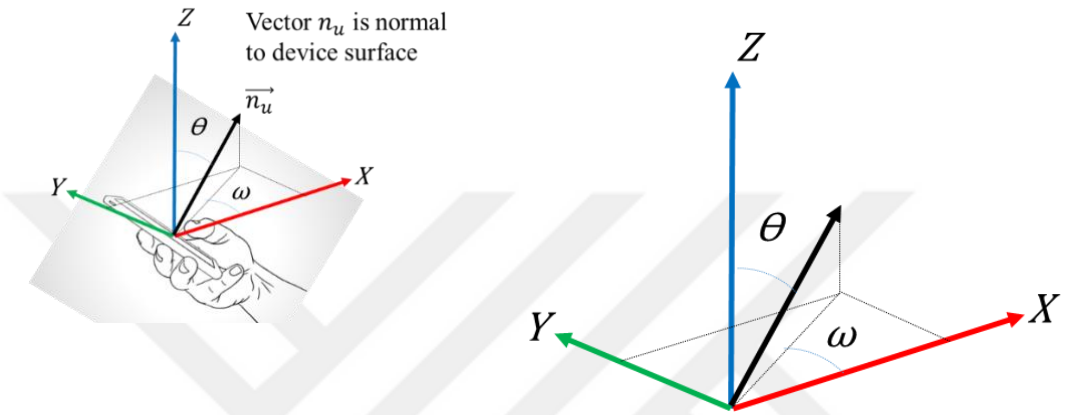

Figure II.4. Polar and azimuth angles [35].

The position vectors defining the locations of the Access Point (AP) and the user, respectively, are denoted by the letters x_a, y_a, z_a, and x_u, y_u, z_u.

The polar angle can be modelled using a truncated Laplace distribution [35], with a mean and standard deviation of 41° and 9°, respectively, and a value that falls between [0, 180°]. The azimuth angle follows a regular distribution [35].

2.5. Channel Effects

In VLC systems, extra light sources that interfere with the message signal can also cause signal degradation in addition to noise elements. These mainly fall into two categories [36]:

Natural Sources: These include celestial bodies like the sun and moon. Their bright emissions might interfere with the light beam's encoding of the message. Generally speaking, they increase the number of photons impinging on the Photodetector's (PD) effective area, forcing it to function in its saturation region [37].

Artificial Sources: Artificial light sources such as other Light Emitting Diodes (LEDs), fluorescent lights, and extra light sources in the area can also cause interference.

The distance between the transmitter and receiver also affects the signal. It is necessary to consider factors like Line-of-Sight (LoS) channel gain and Non-Line-, such as reflections from furniture and wall surfaces. However, as the optical power obtained from signals reflected more than once is low, only the signals from the LoS path and the first-order reflected links are typically taken into account [36].

Due to the fact that VLC connections use receivers with surface areas that are often many orders of magnitude greater than the transmission wavelength, they are not subject to the detrimental effects of multi-path fading like RF communication systems are. The VLC channel's susceptibility to interference and shadowing, as well as the implications of the gadget's orientation [15].

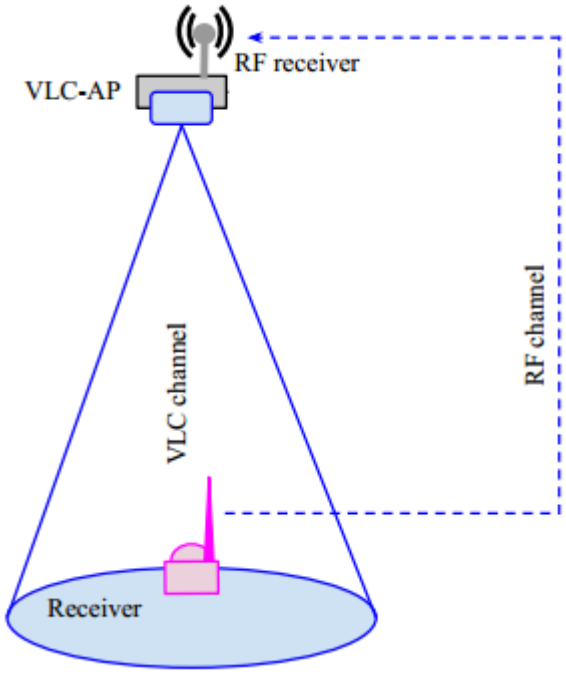

Figure II.5. A duplex VLC transmission system [16].

2.6. VLC System Components

2.6.1. LED

The emission of light in a p-n type LED is achieved through the application of a bias voltage across the p-n junction. The bias voltage facilitates the movement of electrons from the n-junction towards the p-junction, while simultaneously causing holes from the p-junction to migrate to the opposite side. These minority carriers then combine within the depletion layer, also known as the band-gap region, as illustrated in Figure II.6. To enable the recombination of a high-energy electron and a low-energy hole, the excess energy must be released. Consequently, a photon with energy

approximately equivalent to the band-gap energy is emitted when the electron transitions from the conduction band to the valence band [38].

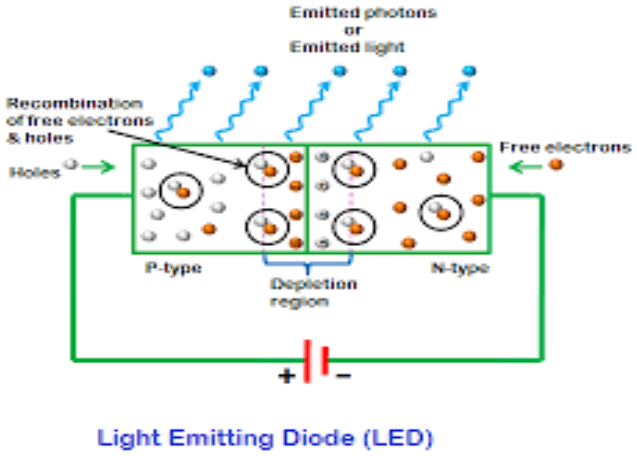

Figure II.6. Recombination across PN junction.

The wavelength of a photon is determined by its energy magnitude and is controllable by the semiconductor material used. The following formula can be used to express the relationship between the band-gap energy and the wavelength of the emitted photon [39]:

$$E_g = hf \tag{II.13}$$

When E_g is the band-gap energy, h is Planck's constant (6.626×10^{-34} J-s), and f is the frequency of the photon that was emitted. The following equation can be used to express this frequency in terms of the photon's wavelength (λ):

$$hf = h(c/\lambda) \tag{II.14}$$

Here, c stands for the speed of light (3×10^8 m/s), and λ stands for the photon's wavelength.

For every electron injected, the ideal LED should emit one photon. The internal quantum efficiency (IQE) or quantum yield is denoted by Equation (II.14) and is

defined as the ratio of the number of photons released to the number of electrons injected at the junction [40][41][42].

Internal quantum efficiency is expressed as

$$\eta_{int} = \frac{N_{p,emit}}{N_{e,inj}} \tag{II.15}$$

where η_{int}, $N_{p,emit}$, and $N_{e,inj}$ stand for, respectively, the number of protons emitted from the active region and the number of electrons injected.

The unit extraction efficiency of an LED is the rate at which all photons in the active region leave the diode. But not all of the photons that are released in the active zone leave the diode because of absorption and other factors. Another crucial factor determining an LED's effectiveness is what is known as the optical efficiency. That is the ratio between photons emitted in the active zone per second and photons radiated into free space per second, as shown in Equation (II.15) [40].

$$\eta_t = \frac{N_{p,air}}{N_{p,emit}} \tag{II.16}$$

where the terms η_t, $N_{p,air}$, $N_{p,emit}$ refer, respectively, to the extraction efficiency, the number of photons released into the atmosphere, and the number of photons radiated in the active region. Thus, by combining Equation (II.14) and Equation (II.15) [42], one can get the external quantum efficiency of an LED:

$$\eta_{ext} = \frac{N_{p,air}}{N_{e,inj}} \tag{II.17}$$

The ratio of the output power to the input power, or the electrical power applied to the LED $P_{elec}^{inj} = VI$ to the emitted photon energy (P_{photon}), is ultimately what determines a device's power efficiency.

$$\eta_P = \frac{P_{photon}}{VI} \tag{II.18}$$

2.6.2. LED Construction

Key factors in LED manufacturing include the selection of materials for the n-type and p-type semiconductors, their physical shape, the design of the device housing, and the arrangement of the light escape path. A typical LED comprises a semiconductor material (referred to as the die or chip), a mounting frame, and an encapsulation material that covers the assembly (see Figure II.7). The LED semiconductor is commonly positioned within a reflector cup attached to the cathode electrode, while the top surface of the chip is connected to the anode electrode using a gold bonding wire. Many of the most intricate designs of junction structures call for two bonding wires—one for each electrode. Different LEDs differ not only in terms of their radiation wavelength, but also in terms of their form, size, and radiation pattern. The housing/lens system's diameter ranges from 2 to 10 millimeters, and semiconductor LED chips can be as large as several square millimeters in size. Although they can also be rectangular, square, triangular, or polygonal, LED bodies most frequently have a hemispherical geometry. The intricate architecture of two well-known LED package designs is seen in Figure II.7. Figure II.7 (a) of the first design shows a typical 5-millimeter LED with a hemispherical lead-frame. In electronic devices, this type of LED is frequently used as an indication bulb [43]. These LEDs have cylindrical and rectangular lens geometries, and their encapsulant system is made of epoxy resins. Conical reflector cups that are soldered to the cathode lead contain a semiconductor die that is firmly in place inside of them. A bonding wire is used to join the anode to the die. The cup reflects any light that the LED's sides may emit, sending

it into the epoxy body. Additionally, a flat part is built into the epoxy dome's foundation, serving as an indicator of the lead polarity. This particular sort of indicator LED typically has a die size of 0.3 millimeters on each side, and the diameter of the lens can range from 2 to 10 millimeters. A high-power GaInN flip chip diode design with an aluminum or copper heat sink slug is shown in Figure II.7. For better heat dissipation, this slug can be soldered onto a printed circuit board. A silicone layer covering the die avoids total internal reflection of the wavefronts that are released and directs them toward the larger plastic lens. The big cathode lead is connected to the die via a gold wire, which is installed on a silicon chip to prevent electrostatic discharge. Although it is not seen in Figure II.7, the anode arrangement in the aforementioned LED design is comparable to the cathode layout but extends in the other direction. Currently, fluorescence microscopy applications that require light choose LEDs with this unique configuration [44].

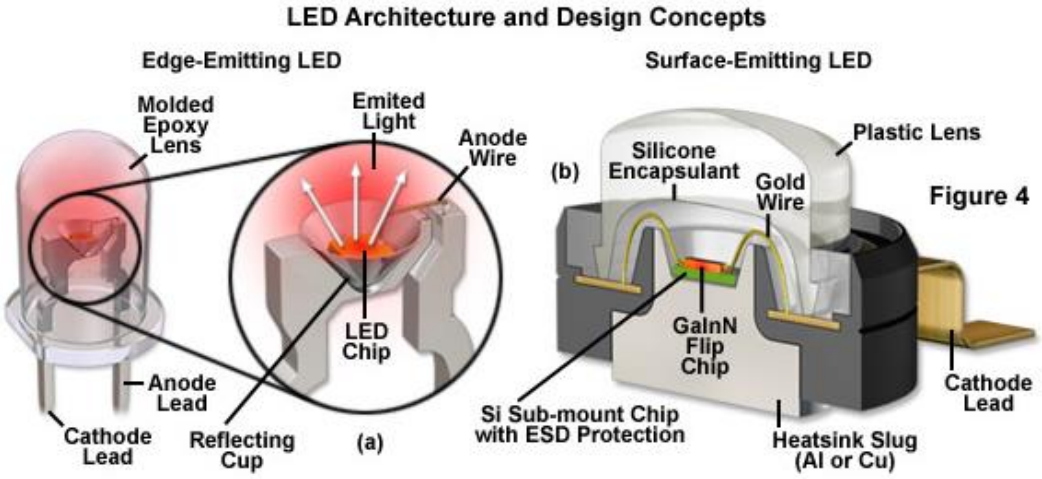

Figure II.7. LED structure.

2.6.3. Channel Impairments

2.6.3.1. Geometrical Loss A_{geo}

Geometrical loss occurs when a light beam diverges from its original direction due to its finite divergence angle. This divergence causes the beam to spread out, and only a fraction of the beam power is captured by the receiver. The geometrical loss is defined as the ratio of the power collected by the receiver to the total power emitted by the light [45]. A_{geo} defines the geometrical loss.

2.6.3.2. Atmospheric Attenuation A_{atm}

Atmospheric attenuation is the reduction in the intensity of an electromagnetic or acoustic signal as it propagates through the atmosphere. It is caused by two main mechanisms: scattering and absorption.

- Scattering occurs when the signal is deflected by particles in the atmosphere, such as air molecules, water vapor, and dust. This causes the signal to spread out and become weaker.
- Absorption occurs when the signal is absorbed by the molecules in the atmosphere. This is more pronounced for certain frequencies, such as those emitted by radar and lidar.

The amount of atmospheric attenuation depends on the frequency of the signal, the temperature and humidity of the atmosphere, and the presence of clouds or other particles, which typically has a value of 0.5 dB [45].

As the optical signal passes through fog and smoke particles, the light is both absorbed and experiences Mie scattering [46], leading to further attenuation of the beam in fog (A_{fog}). A_{fog} attenuation is depends on channel visibility (V_{is}) [47], which

is the distance at which two objects can be just barely distinguished. V_{is} is typically measured in kilometers. Two well-known models for A_{fog} are the Kim model and the Kruse model. The equation for these models is [48]

$$A_{fog} = \frac{3.912}{V_{is}} \left(\frac{\lambda}{550\text{nm}} \right)^{-q} \tag{II.19}$$

where V_{is} is in units of km.

The Kim model defines the attenuation coefficient q as follows:

$$q = \begin{cases} 1.6 & V_{is} > 50m \\ 1.3 & 6 < V_{is} < 50 \\ 1.6V_{is} + 0.34 & 1 < V_{is} < 6 \\ V_{is} - 0.5 & 0.5 < V_{is} < 1 \\ 0 & V_{is} < 0.5m \end{cases} \tag{II.20}$$

Beer-Lambert law gives the relation between the total attenuation due to the scattering of light β_λ and A_{fog} absorption [49]

$$\beta_\lambda = -\frac{10 \log A_{fog}}{4.343\, L} \tag{II.21}$$

L stands for the link distance. Fog can be thick, with low visibility ($V_{is} < 0.1$m), medium ($0.1\text{m} < V_{is} < 1\text{m}$), or thin ($V_{is} > 1$m).

2.6.3.3. Additional Losses

Losses can result from misalignment, equipment, or other unidentified reasons are included in this category of attenuation [47]. In FSO systems, rain also causes a loss, though it is not as big as fog or smoke [47]. Rain, however, is a significant attenuation factor in VLC systems. [45] provides the received power with respect to transmit power Pt and all losses.

$$P_r = P_t - A_{geo} - A_{atm} - A_{fog} - A_{misc} \tag{II.22}$$

The link electrical signal-to-noise ratio (SNR) depends on total noise variance at the receiver σ^2, and photodiode responsivity R [45]

$$SNR = \frac{(RP_r)^2}{\sigma^2} \quad \text{(II.23)}$$

System BER for the no fading channel is given by [45]:

$$BER = Q\left(\sqrt{SNR}\right) \quad \text{(II.24)}$$

where Q(·) denotes the Gaussian Q function defined as

$$Q(x) = \int_x^{\infty} \exp(-t^2/2)\, dt \quad \text{(II.25)}$$

The optical link propagation mechanism in the VLC system is also LOS, where the link experiences very little or no fading but does encounter the following attenuations:

1. The geometrical loss in FSO, which is given as [50], is similar to free space path loss (FSPL).

$$FSPL = 20 \log\left(\frac{4\pi L}{\lambda_{VLC}}\right) \quad \text{(II.26)}$$

where λ_{VLC} is the VLC signal wavelength.

2. Rain attenuation A_{rain} - Is the main cause of VLC link unavailability, and is caused by the absorption phenomena when the light energy is absorbed by rain [51]. A_{rain} in dB for VLC spectrum is given by:

$$A_{rain} = 1.076L(R)^{2/3} \quad \text{(II.27)}$$

where R is the precipitation rate in mm/h.

3. Atmospheric turbulence (AT) is a random variation in the refractive index of the channel usually due to heat and exhaust gasses. This variation can cause the wavefront of an optical beam to be distorted, which can lead to signal loss and fading. The size of turbulence eddies can range from millimeters to meters [29]. Turbulence changes slowly, the channel induced by AT typically has a coherence time between 1 and 10 ms. is a slow varying fading channel, with a temporal coherence time of 1 to 10 milliseconds [52]. Figure II.8 illustrates the effect of AT on the VLC signal.

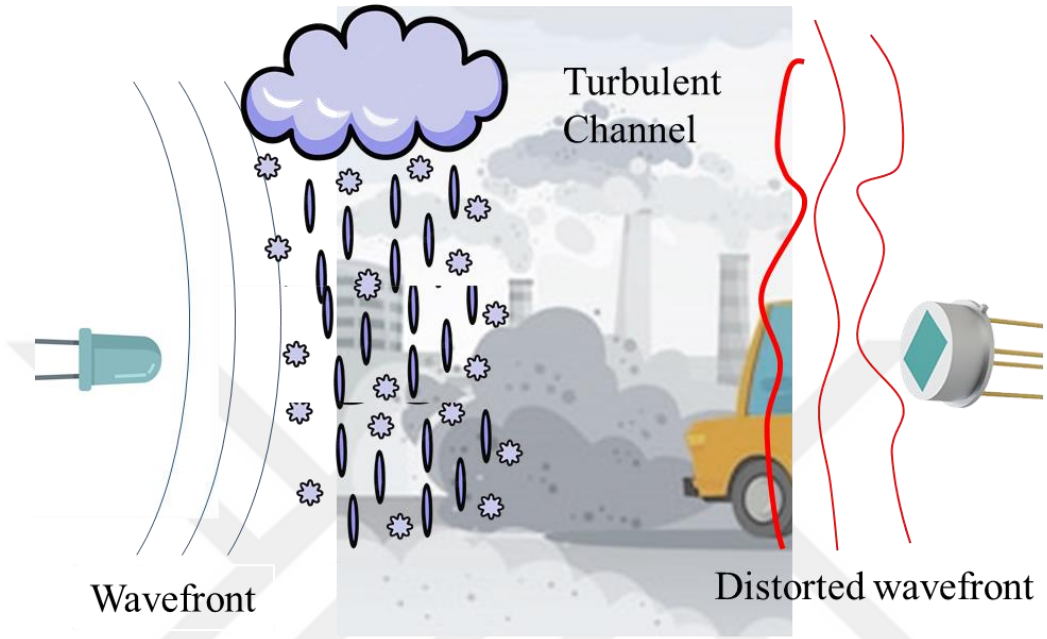

Figure II.8. Turbulent channel at a fixed time.

Channel correlation radius ρ_c, can be calculated as [53]:

$$\rho_c \approx d_0^2/\pi\rho_0 \tag{II.28}$$

where $d_0 \approx \sqrt{\lambda_{FSO} L}$ is correlation length and $\rho_0 = (1.46 k_{FSO}^2 C_n^2 L)^{-3/5}$ is spatial coherence radius [53]. $k_{FSO} = 2\pi/\lambda_{FSO}$ is the wavenumber and C_n^2 is the index-of-refraction structure.

2.6.4. Optical Detectors

2.6.4.1. Photodiodes

Photodiodes are the most common type of optical detectors used in VLC systems. They operate based on the principle of the photovoltaic effect, generating a

photocurrent proportional to the incident light intensity. Photodiodes can be further classified into PIN photodiodes, avalanche photodiodes (APDs), and phototransistors [40][54].

2.6.4.2. PIN Photodiodes

PIN photodiodes are frequently employed in VLC systems. They have high responsivity, wide bandwidth, and low noise. They offer a linear response to the incident light and are suitable for moderate-to-high-speed VLC applications.

Modulation Equation: The modulation equation represents the process of encoding information onto the optical signal transmitted by the VLC system. One common modulation technique used in VLC is pulse amplitude modulation (PAM), where the amplitude of the optical signal is varied according to the input data.

Let's assume we have a binary data stream, where '1' represents the presence of a signal and '0' represents the absence. The modulated optical signal can be represented as:

$$s(t) = (A + dA)m(t) + \cos(2\pi f_c t) \quad \text{(II.29)}$$

In the above equation:

- $s(t)$ represents the modulated optical signal as a function of time.
- A is the average amplitude of the optical signal.
- dA represents the amplitude variation according to the input data.
- $m(t)$ is the binary data stream.
- f_c is the carrier frequency.

Demodulation Equation: The demodulation equation represents the process of extracting the original data from the received optical signal. In VLC systems, PIN

diodes are used as photodetectors to convert the optical signal into an electrical current [55].

Let's assume the received optical signal is given by:

$$R(t) = (A + dA)m(t)\cos(2\pi f_c t) + N(t) \quad \text{(II.30)}$$

In the above equation:

- $R(t)$ represents the received optical signal as a function of time.
- $N(t)$ represents the additive noise.

The demodulation process involves multiplying the received signal by a local oscillator signal (cosine wave at the carrier frequency) and then low-pass filtering to remove high-frequency components. This process is equivalent to envelope detection. The resulting signal can be expressed as:

$$Y(t) = R(t)\cos(2\pi f_c t + \phi) \quad \text{(II.31)}$$

Where ϕ represents the phase shift between the transmitted and received signals.

To recover the original data, the demodulated signal is typically thresholded. If the amplitude of the demodulated signal is above a certain threshold, it is interpreted as '1', otherwise as '0' [56].

2.6.4.3. Avalanche Photodiodes (APDs)

APDs are high-gain photodetectors that incorporate an avalanche multiplication mechanism. They provide increased sensitivity and are commonly used in low-light environments or long-range VLC systems. APDs offer improved signal-to-noise ratio (SNR) and enhanced receiver sensitivity compared to PIN photodiodes. Figure II.9 shows the APD structure.

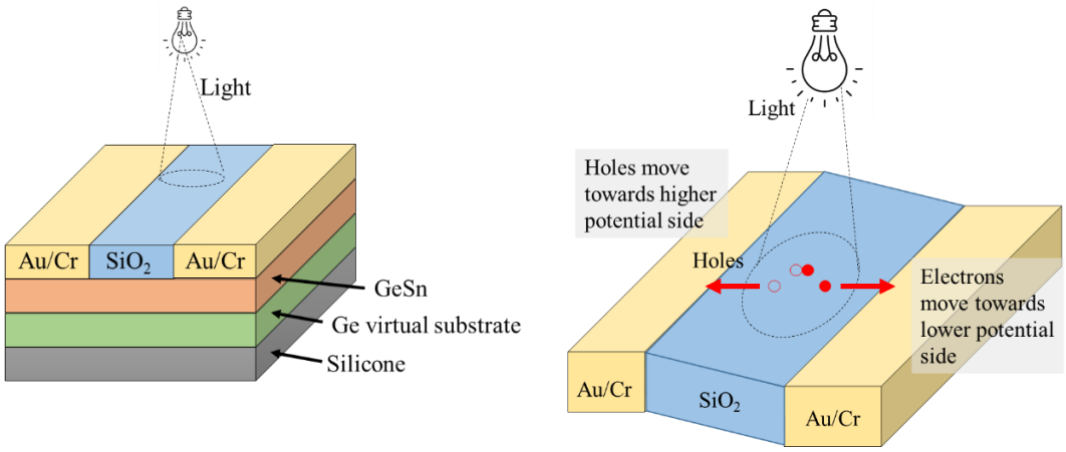

(a) (b)

Figure II.9. Avalanche photodiodes structure and operation

2.6.4.4. Phototransistors

Phototransistors are bipolar junction transistors with a light-sensitive base region. They exhibit higher sensitivity than PIN photodiodes but have a slower response time. Phototransistors are suitable for low-cost and low-speed VLC applications.

2.6.5. Filters

Filters play a pivotal role in enhancing the quality and efficiency of VLC systems. By performing noise reduction and signal shaping, they ensure that the data transmission and reception are reliable. In addition, by facilitating the multiplexing and demultiplexing of signals, filters effectively increase the overall data capacity of VLC systems [45].

The primary functions of filters in VLC systems can be summarized as follows:

1. Noise Reduction: Filters eliminate or reduce the noise in the system, ensuring a clean signal transmission, which is crucial for achieving reliable communication.
2. Signal Shaping: Filters assist in shaping signals to avoid intersymbol interference that can lead to errors in the decoded data.
3. Multiplexing/Demultiplexing: Filters enable the multiplexing and demultiplexing operations, which are crucial for transmitting multiple signals over the same channel simultaneously.

Specific types of filters used in VLC systems include band-pass, low-pass, and high-pass filters [55].

2.6.5.1. Low-Pass Filters (LPF)

These filters allow signals with a frequency lower than a certain cutoff frequency to pass through and attenuate frequencies higher than the cutoff frequency. The transfer function of a simple first-order (RC) low-pass filter is given by:

$$H(s) = \frac{V_{out}(s)}{V_{in}(s)} = \frac{1}{1 + sRC} \tag{II.32}$$

where s is the complex frequency, R is the resistance, and C is the capacitance. Figure II.10 shows the frequency response of LP filter.

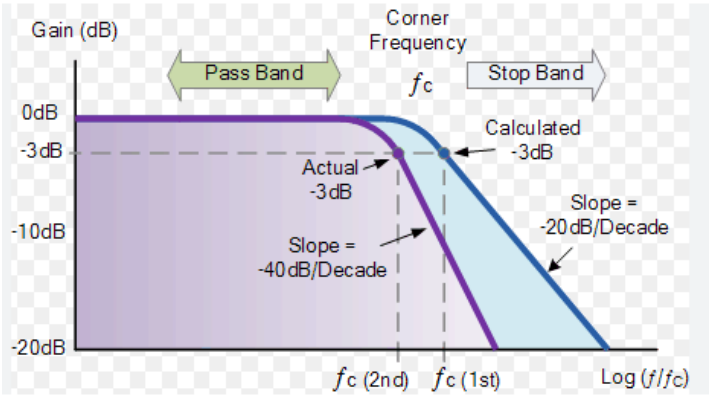

Figure II.10. Frequency response of LP filter.

2.6.5.2. High-Pass Filters (HPF)

These filters do the opposite of LPFs, attenuating frequencies lower than a certain cutoff frequency and allowing frequencies higher than the cutoff to pass. Figure II.11 shows the frequency response of HP filter. The transfer function of a simple first-order (RC) high-pass filter is:

$$H(s) = \frac{V_{out}(s)}{V_{in}(s)} = \frac{sRC}{1 + sRC} \tag{II.33}$$

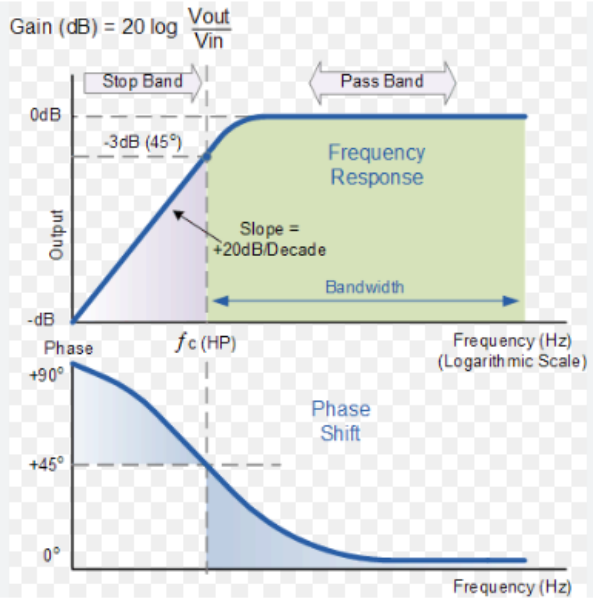

Figure II.11. Frequency response of HP filter.

2.6.5.3. Band-Pass Filters (BPF)

These filters allow signals within a specific frequency range to pass through and attenuate frequencies outside this range. A band-pass filter can be seen as a combination of high-pass and low-pass filters. Figure II.12 shows the frequency response of BP filter

The transfer function of a simple band-pass filter is [45][57].

$$H(s) = \frac{V_{out}(s)}{V_{in}(s)} = \frac{sRC}{s^2R_2C_2 + sRC + 1} \quad \text{(II.34)}$$

In each of these functions, the value of *s* (complex frequency) can be replaced by $j\omega$, where j is the imaginary unit and ω is the frequency of the input signal.

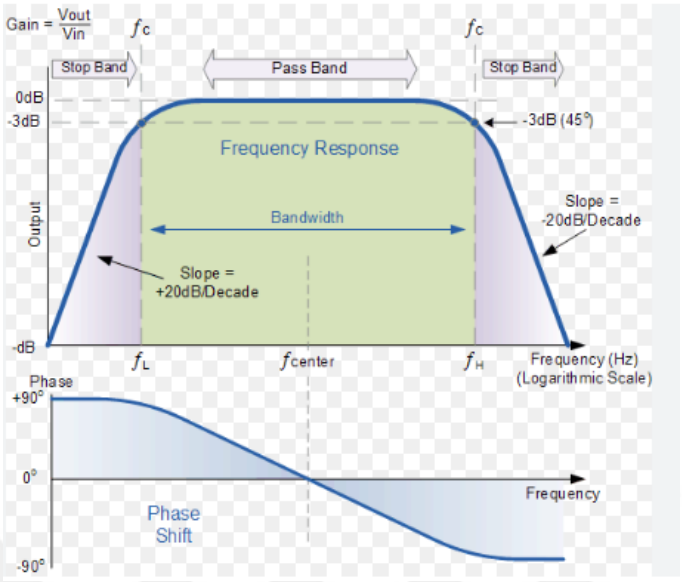

Figure II.12. Frequency response of BP filter.

2.7. Noise Types in PIN Photodetectors

Noise in optical detectors can degrade the system's performance. Important noise characteristics include dark current noise, shot noise, and thermal noise. Minimizing noise sources is crucial for achieving high-quality data transmission.

Noise in photodetectors refers to the random variations of brightness or color information in images. It is an unwanted signal that can cause significant performance issues in photodetection systems.

2.7.1. Shot Noise

In photodetectors, shot noise arises due to the discrete nature of the electric charge, and it's proportional to the square root of the average number of detected photons [58]. Shot noise in a photodetector arises due to the discrete nature of the

electric charge. Each photoelectron is counted discretely, and since the occurrence of photoelectrons is a random event, it creates fluctuations in the photocurrent. The root mean square (RMS) current noise due to shot noise (I_shot) in a photodetector is given by the following equation:

$$I_{shot} = \sqrt{2eIB} \quad \text{(II.35)}$$

where *e* is the elementary charge (~1.602 x 10-19 Coulombs),

I is the DC current (average current) in Amps, and

B is the bandwidth in Hz.

This equation tells us that shot noise increases with the square root of the average current and the bandwidth.

Shot noise is fundamentally unavoidable but is not always the limiting noise source in a photodetector. Other noise sources such as thermal noise or $1/f$ noise may dominate depending on the operating conditions. Shot noise has a white noise spectral density (flat with frequency) and is independent of temperature.

2.7.2. Thermal Noise

This type of noise arises due to the random motion of charge carriers in a conductor. The noise is dependent on temperature, the resistance of the conductor, and the bandwidth over which it's measured [59]. Thermal noise, also known as Johnson-Nyquist noise, arises due to the random motion of charge carriers (usually electrons) in a conductor (the photodiode, in this case) which happens due to the thermal agitation. The root mean square (RMS) voltage due to thermal noise ($V_{thermal}$) in a resistor is given by the following equation:

$$V_{thermal} = \sqrt{4kTRB} \quad \text{(II.36)}$$

where:

k is Boltzmann's constant (~1.38064852 × 10^{-23} Joules per Kelvin),

T is the absolute temperature in Kelvin,

R is the resistance in Ohms, and

B is the bandwidth in Hz.

This equation tells us that thermal noise increases with the square root of the temperature, resistance, and bandwidth. It's important to note that the spectral density of thermal noise is constant and does not depend on frequency (white noise).

In terms of current, the current noise due to thermal fluctuations ($V_{thermal}$) in a resistor can be given as:

$$I_{thermal} = \sqrt{4kTGB} \quad \text{(II.37)}$$

where *G* is the conductance, which is equal to 1/*R*.

2.7.3. Dark Current Noise

Dark current is the current that flows through a photodetector even in the absence of light. Dark current noise is proportional to the square root of the average dark current [60]. Dark current in photodetectors refers to the electrical current that can flow even when no photons are entering the device. It's typically caused by thermal energy or unwanted incident light. Similar to shot noise, dark current noise is a statistical process and follows a similar equation. The root mean square (RMS) dark current noise (I_{dark}) can be calculated by:

$$I_{dark} = \sqrt{2eI_dB} \quad \text{(II.38)}$$

where:

e is the elementary charge (~1.602 x 10^-19 Coulombs),

I_d is the average dark current (DC) in Amps, and

B is the bandwidth in Hz.

This equation tells us that dark current noise increases with the square root of the average dark current and the bandwidth. One of the ways to reduce dark current (and consequently, dark current noise) is to cool the photodetector, as dark current is typically heavily temperature dependent.

2.7.4. Quantum Noise

This is the noise associated with the quantization of light, i.e., the fact that light comes in discrete packets of energy (photons) [61]. Quantum noise in photodetectors arises due to the inherent uncertainty and randomness associated with the quantization of light into discrete packets of energy, known as photons. In the context of photodetectors, this often refers to the shot noise associated with the statistical fluctuations in the number of photoelectrons generated, as the arrival times of individual photons follows a Poisson process.

The standard quantum limit (SQL) or shot noise limit (SNL) is the fundamental limit of precision set by quantum mechanics. For light of a particular intensity and frequency, the shot noise or quantum noise power (P_noise) is given by:

$$P_{noise} = \sqrt{2hvPB} \tag{II.39}$$

where h is Planck's constant (6.626×10^{-34} J-s), v is the frequency of light in Hz, P is the power of the light in Watts, B is the bandwidth in Hz.

This equation tells us that quantum noise increases with the square root of the light power and the bandwidth.

2.7.5. 1/f Noise

Also known as flicker noise, this noise impacts the low-frequency performance of PIN photodetectors [62].

2.8. Performance Characteristics

2.8.1. Responsivity

Responsivity refers to the ratio of the detector's electrical output to the incident optical power. It quantifies the detector's sensitivity and is an essential performance parameter for optical detectors.

Responsivity (R) of a photodetector is a key parameter that indicates how much electrical output you get for a given amount of optical input. It's typically measured in Ampere per Watt (A/W). The mathematical relation for responsivity can be written as follows:

$$R = I_{ph}/P \tag{II.40}$$

where R is the responsivity (A/W), I_{ph} is the photocurrent, the electrical output of the detector, which is measured in Amperes (A), and P is the incident optical power, which is measured in Watts (W).

The photocurrent, I_{ph}, is produced when incident light (with power P) is absorbed and creates electron-hole pairs. These pairs are separated by an electric field, which generates the photocurrent. Therefore, a higher responsivity means that the detector generates more current for a given amount of light, making it more sensitive.

2.8.2. Bandwidth

The bandwidth of an optical detector defines its ability to respond to rapid changes in the incident light. Higher bandwidth allows for higher data transmission rates in VLC systems.

In the context of optical detectors and Visible Light Communication (VLC) systems, bandwidth is an essential parameter that describes how fast the system can respond to changes in the incident light. The concept of bandwidth is important because it limits the data rate, or speed, at which information can be transmitted.

Let's denote the bandwidth by the symbol '*B*'. According to Nyquist's theorem, which is fundamental in information theory and telecommunications, the maximum data rate or capacity '*C*' of a channel can be determined using the following equation:

$$C = 2B \log_2(M) \tag{II.41}$$

where *B* is the bandwidth (in Hz), and *M* is the number of distinct signal levels (the number of different states the signal can represent).

The factor '2' comes from the fact that the bandwidth *B* is usually defined as the range of frequencies from DC (0 Hz) up to some maximum frequency, and each of these frequencies can carry two bits of information per cycle (one for the positive half cycle and one for the negative half cycle).

If binary modulation is used (where each signal can only represent two states, such as '0' or '1'), the number *M* would be 2, and the maximum data rate would simplify to [56]:

$$C = 2B \log_2(2) = 2B \tag{II.42}$$

III. SYSTEM MODELING AND RESULTS

3.1. Introduction

Visible light communication (VLC) is a low latency high throughput communication scheme which is being considered for vehicular communication in 6G networks. For this purpose it is important to study VLC using simulation and experimental studies.

This chapter presents a simulation model for VLC systems that was built using OptiSystem and MATLAB. The model can be used to study the performance of VLC systems in a variety of channel configurations, such as data rate, noise level and transmitter antenna size. and to design and optimize VLC systems.

The chapter begins with a description of the simulation model, including the OptiSystem and MATLAB components. The chapter then presents the results of several simulation studies, which demonstrate the performance of the model.

3.2. VLC System Simulation

Visible light communication was built using OptiSystem for investigate its performance under variety of channel configurations. Figure III.1 shows the system under investigation.

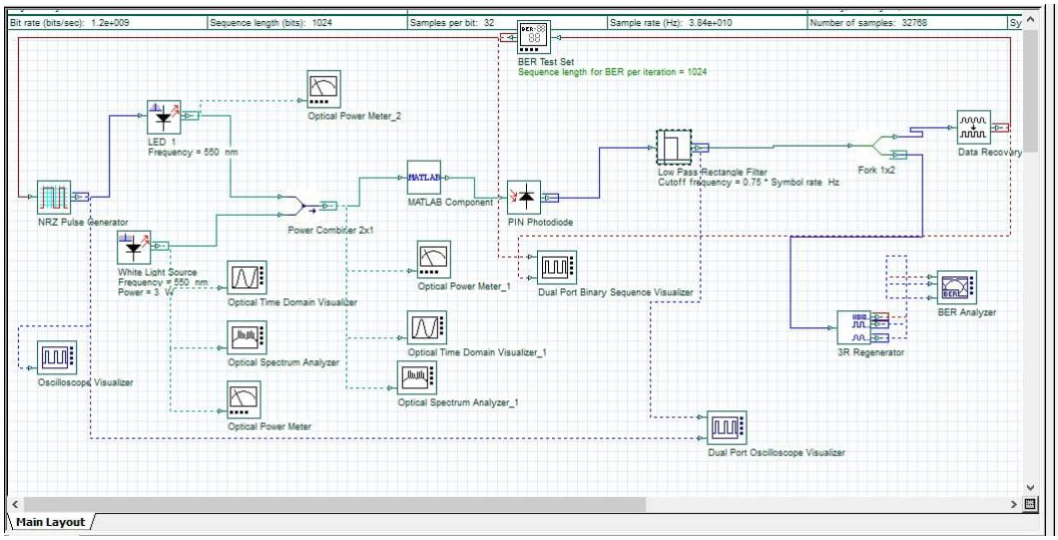

Figure III.1. OptiSystem model.

The transmitter section of the VLC system consists of

- A pseudorandom binary sequence (PRBS) generator that generates random bit to be transmitted.
- A non-return-to-zero (NRZ) pulse generator that converts a digital signal into pulses. The NRZ pulses have two levels, representing the binary values 0 and 1. The pulses in an NRZ signal do not return to the baseline level between successive pulses, which is why it is called "non-return-to-zero." NRZ pulse generators are commonly used in visible light communication (VLC) systems. This is because NRZ signals have more energy than return-to-zero (RZ) signals, which makes them more robust to noise. Additionally, NRZ signals are easier to demodulate than RZ signals, which makes them a good choice for VLC systems.
- LED that emits light at a wavelength of 550 nanometers (green color) and has a modulation bandwidth of 10 THz to transfer the signal from electrical domain

to optical domain. These parameters can be easily adjusted to change the data rate, wavelength, or other characteristics of the system.

- Ambient light is the main cause of interference in VLC systems. This noise is generated by fluorescent lamps and other light sources. White light source was place with different power level to introduce the noise effect within the power combiner.

A MATLAB component were added to simulate the channel performance as will describe later.

The receiver section of the VLC system consists of a PIN photodiode, a low-pass Bessel filter, and data recovery.

The PIN photodiode converts the received optical signal into an electrical signal.

- Low-pass Bessel filter removes the undesired components of the received signal, such as the carrier frequency and the harmonics of the carrier frequency.
- Data recovery recovers the original bits through Analog to digital convertor (ADC).
- The 3R generator is an extra output port created to forward the data to calculate the BER. The system uses the Data Recovery unit of OptiSystem and regenerates the pulse sequence to calculate the BER. Its output can be feed directly to Eye diagram analyzer for performance investigation.

Table III.1 summarizes the simulation parameters.

Table III.1. Main component configuration

Components	**Values**	**Units**
Bit rate	10	kbps
Modulation	NRZ-OOK	
Optical source (LED) frequency	550	nm
Optical source (LED) bandwidth	1	MHz
Optical background noise frequency	50	Hz
Optical background noise power	36	W
Transmission channel	Matlab modeling	
Distance	10	cm
Modulation constellation	Up to 64-QAM	Up to 256-QAM
FEC	BCC	LDPC
Rectangular optical filter wavelength	450	nm
Rectangular optical filter bandwidth	1	MHz
PIN photo-detector Responsivity	1	A/W
Low pass Bessel filter cut off frequency	0.75 times bit rate	Hz
Channel attenuation	0.008	dB/km

3.3. VLC Channel

Matlab code was written to model the VLC channel based on equations described in Chapter II. Figure III.2 and Figure III.3 show the flow chart for the code.

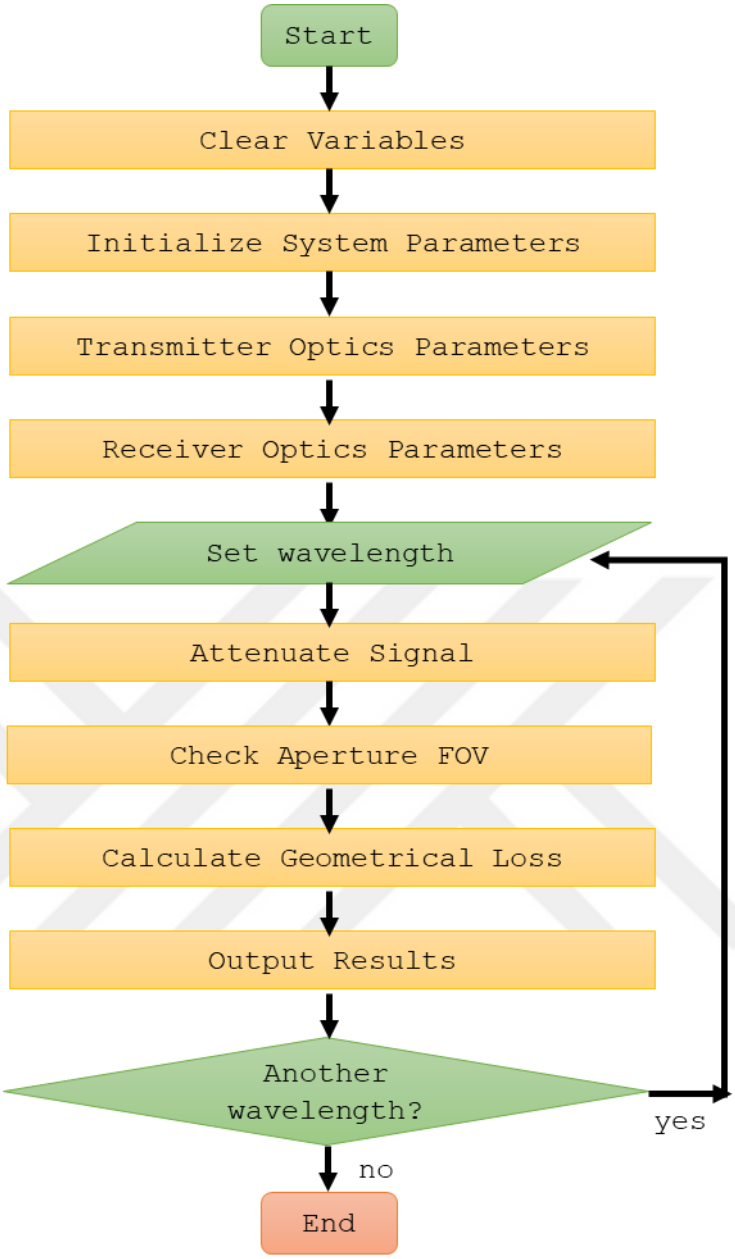

Figure III.2. Matlab model flowchart.

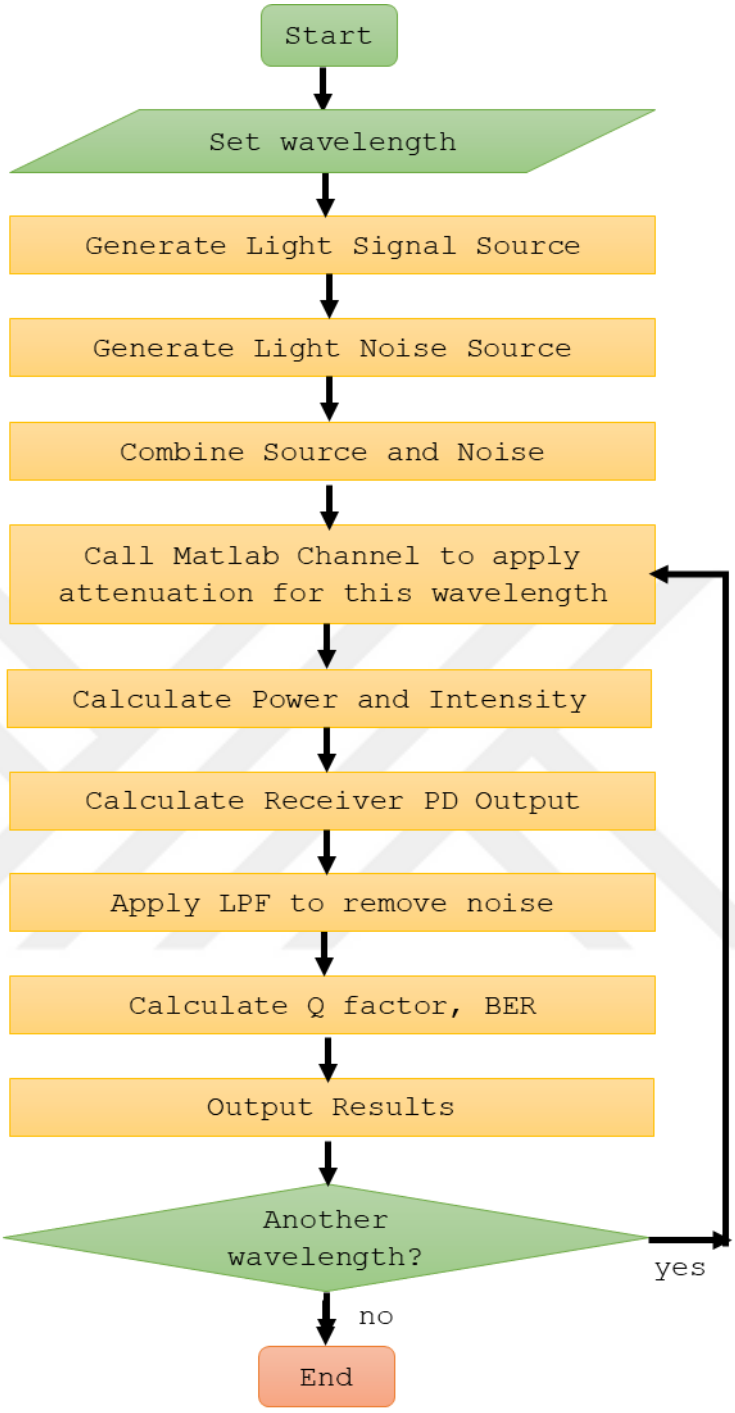

Figure III.3. OptiSystem model flowchart.

3.4. OptiSystem Analysis Tools

In studying the performance of the VLC system using the OptiSystem model, we study the effects of the parameters bit rate value, link distance, as well as the effect of noise. To ascertain the quality of the communication link, the following tools are used. These tools are available from the OptiSystem program.

3.4.1. Eye Diagram and Q Factor

The eye diagram graph has been used since the beginning of communication to visually show the noise margin available in the signal. The eye diagram is formed by repeatedly superimposing traces of the received pulse shape. As the received bit is sometimes a “0” and sometimes a “1”, the middle of the graph which corresponds to the sampling instant for demodulation will sometimes have a low voltage corresponding to an information bit “0”, often called the Level 0 value and sometimes a higher voltage corresponding to a “1”, called Level 1 value. Repeated traces of the pulse will show a figure that looks like an eye with the top lid of the eye corresponding to traces where a 1 was sent and the bottom lid to traces where a 0 was sent, as shown in Figure III.16. Figure III.4 illustrates some of the parameters which can be measured on an eye diagram which give users an idea about the quality of the signal being analyzed.

The eye diagram can give valuable information about the quality of the signal. Since Level 1 and Level 0 values will depend on optical link distortions and noise introduced through the electronic system, the value for each bit will be a random variable. Let μ_0 and σ_0 represent the mean and standard deviation of Level 0 values and μ_1 and σ_1 represent the mean and standard deviation Level 1 values, measured at

the middle of the eye. The further apart these levels are, the lower the BER will be for the signal. When there is noise the variance is high so that the lowest Level 1 values are close to the highest Level 0 values, in this case “the eye is closed” in the eye diagram. If the two levels are always well separated, it is said that “the eye is open”.

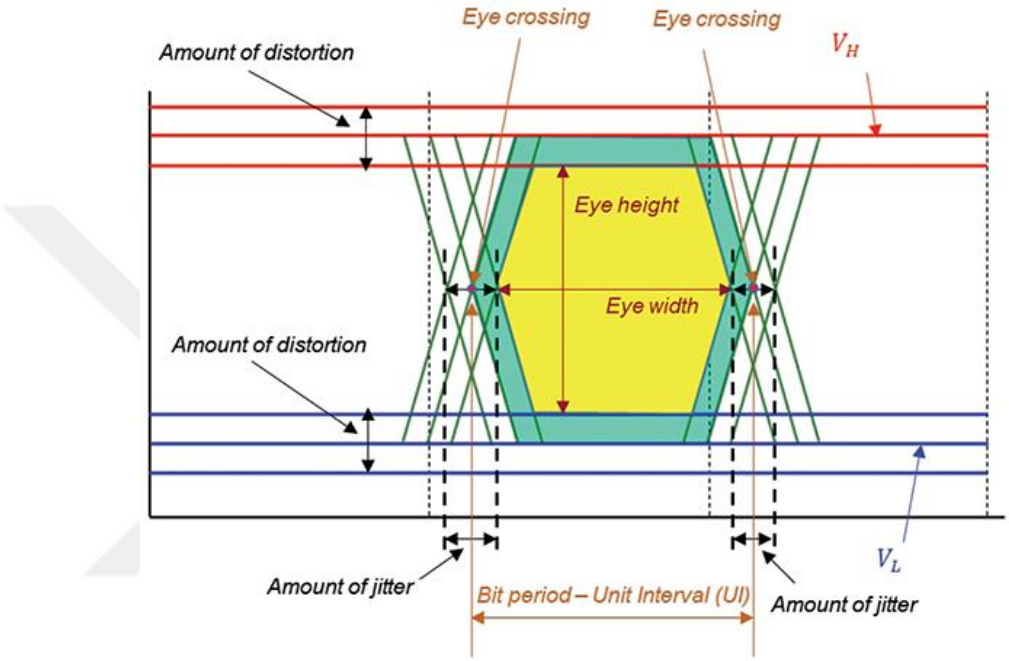

Figure III.4. Eye diagram [63].

The Eye Height (EH) parameter tracks the lower end of Level 1 and the upper values for Level 0: EH= $\mu_1 - \mu_0$ can be used to measure the BER.

$$EH = (\mu_1 - 3\sigma_1) - (\mu_0 + 3\sigma_0) \quad \text{(III.1)}$$

Another way to measure this is to calculate the Extinction Ratio (ER) which is typically expressed in dB as below

$$ER(dB) = 10\log_{10}\left(\frac{\mu_1}{\mu_0}\right) \quad \text{(III.2)}$$

Another measure which is often used to measure and track the quality of the optical link is the Quality Factor or Q Factor. The Q factor is defined as

$$Q = \left(\frac{\mu_1 - \mu_0}{\sigma_0 + \sigma_1}\right) \quad \text{(III.3)}$$

The Q factor is similar to signal to noise ratio, as the numerator will be higher if the two signals levels are far apart, which happens when signal power is high; and the denominator will be higher if the noise levels are high, leading to large variability in the Level 0 and Level 1 values. This factor also incorporates the effect of nonlinear degradation of the light signal due to diffraction, reflection and so on.

The eye diagram can always be used to measure timing errors. For this reason the time at which the signal crosses the midpoint between Level 0 and Level 1 is measured, it is known as the level crossing time. In a single eye diagram, there are two level crossing times, the first is at the beginning of the pulse and the second at the end. Both these crossing times are random variables. Let T_{cross1} and σ_{cross1} represent the mean and standard deviation of the first crossing time and T_{cross2} and σ_{cross2} represent the mean and standard deviation of the second crossing time.

The standard deviation of all crossing times can be calculated, this is known as the Eye Jitter.

The Eye Width (EW) gives the width of the pulse shape. Lower signal quality generally reduces the eye width.

$$EW = (\mu_{cross1} - 3\sigma_{cross1}) - (\mu_{cross0} + 3\sigma_{cross0}) \quad \text{(III.4)}$$

There are other measurements and calculations that can be found using the eye diagram [63][64][65]. This work will focus on the Quality factor as performance metrics for investigation and comparison purpose.

3.4.2. BER Analyzer

Since throughput is the fundamental measure of a communication link, the BER gives a good way to study the VLC link. The BER is a statistic, it is the number of errors that occur in the bit sequence during communication. The BER of a signal in OptiSystem can be measured using the BER analyzer. The BER is a measure of the number of errors that occur in the bit sequence during communication. The BER analyzer can be connected to the VLC system in two ways:

(a) All three input ports of the BER analyzer can be connected directly to the regenerators at the receiver side.

(b) The top two input ports of the BER analyzer can be connected to the PRBS generator and NRZ pulse generator, and the lower input port can be connected to the regenerators at the receiver side.

The BER analyzer tool outputs both the BER and the maximum Q-factor of a signal. The Q-factor is defined above, it gives a measure of the quality of the link. The BER denotes how many errors occur in the bit sequence during communication. The Q-factor and BER values are affected by many parameters in the VLC system, such as the bit rate value, link distance, wavelength, and bandwidth of the LED.

3.5. System Parameters

The OptiSystem model first generates random bits. Figure III.5 is a trace of 20 random bits sent. Each bit is mapped to a NRZ pulse, Figure III.6 shows the NRZ signals. Because the NRZ pulse shape is a square pulse 1 for bit 1 and no pulse for bit 0, the two plots look very similar.

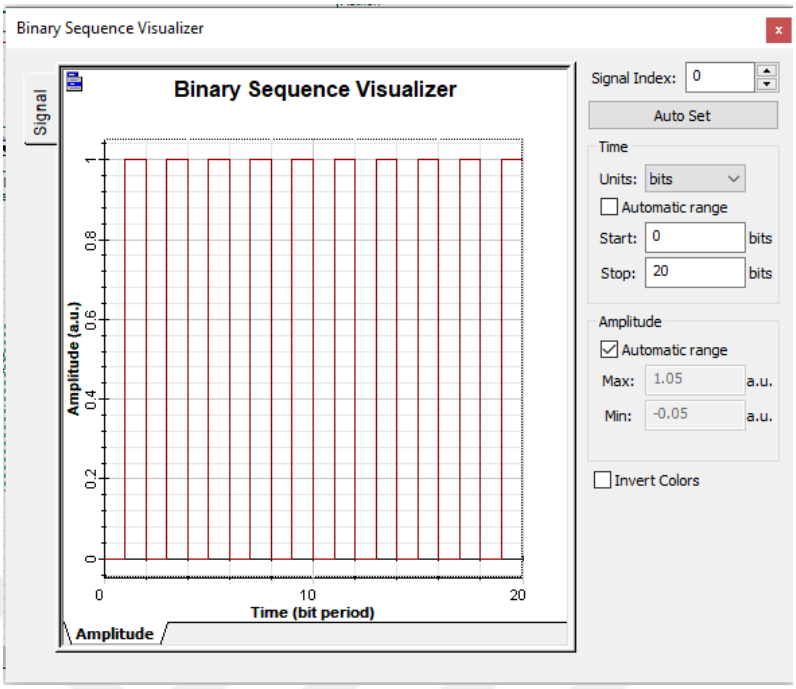

Figure III.5. Random bits.

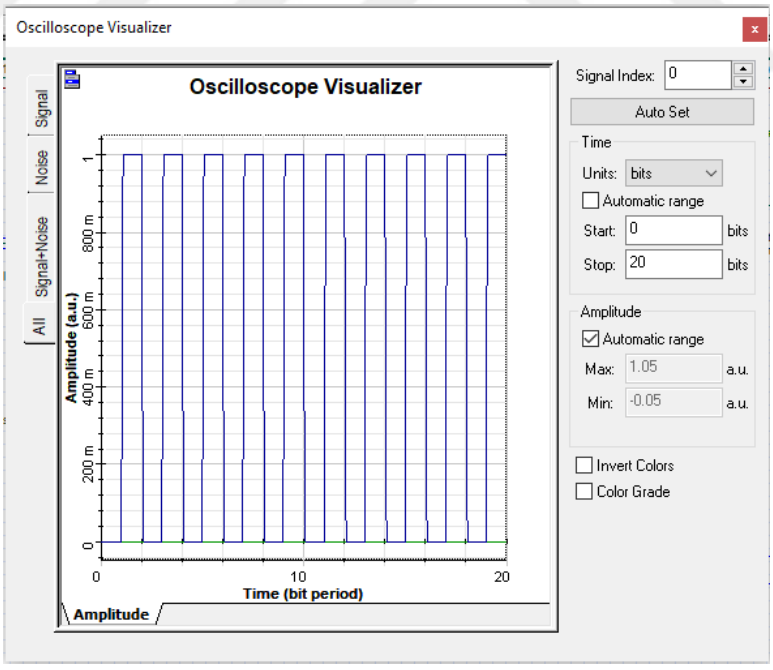

Figure III.6. NRZ symbols.

To investigate the LED frequency response and time domain characteristics as well as the LED power. Figure III.7 and Figure III.8 show the LED frequency and time response, respectively.

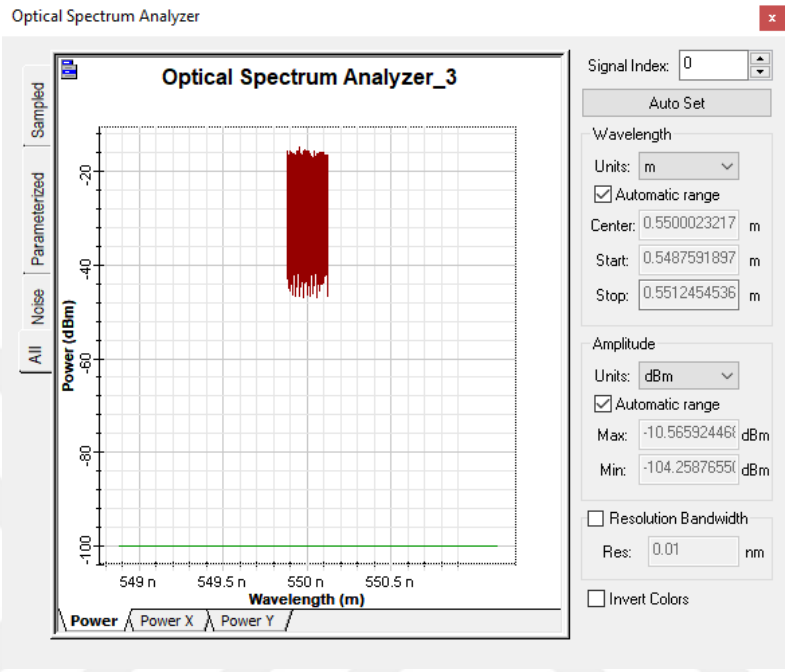

Figure III.7. LED source frequency response.

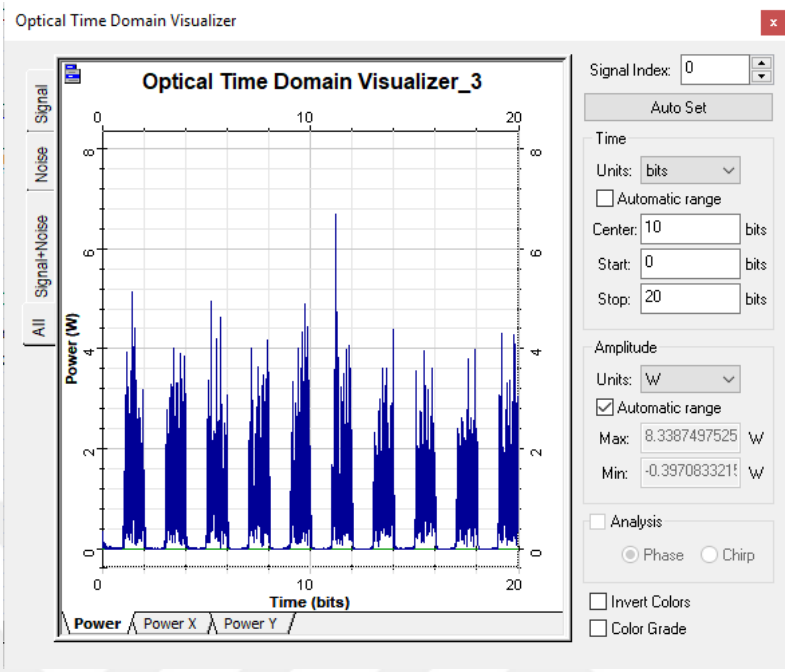

Figure III.8. LED source time response.

The transmit power of the LED is set to various values during simulations. Figure III.9 illustrates the power meter user interface which shows the transmit power of the LED.

Figure III.9. Power meter for LED.

The system performance will be studied at different noise levels. Power meter reading for the white light source at different set power were illustrated in Figure III.10. The interface gives the total power of the signal emitted by the LED in Watts and dBm.

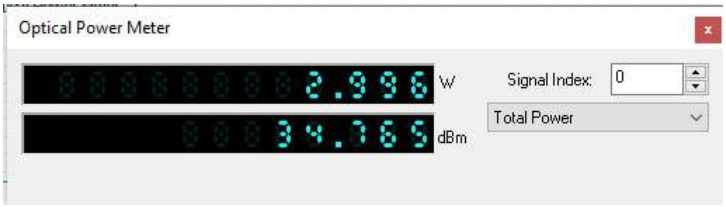

(a) 3W

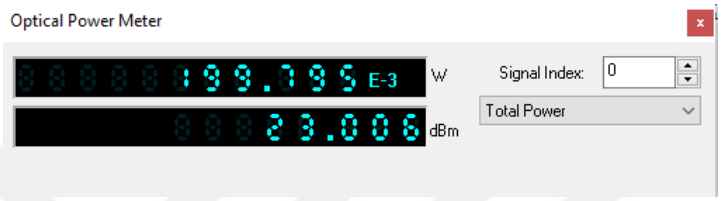

(b) 0.2W

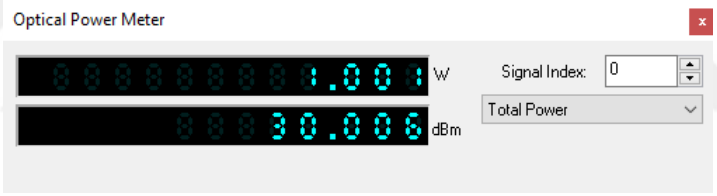

(c) 1W

Figure III.10. White light source power reading (a) 3 W (b) 0.2 W (c) 1 W.

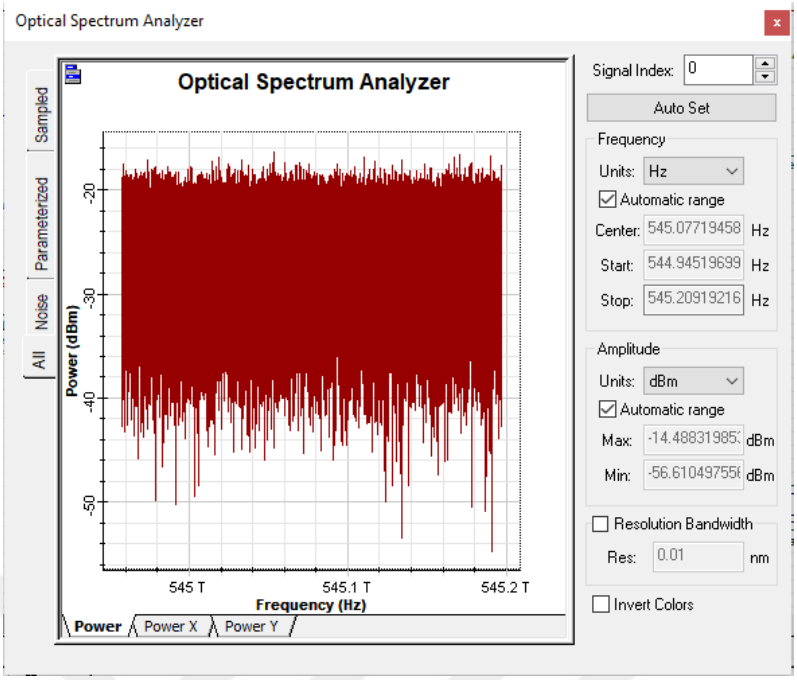

Figure III.11. Frequency response of the white light source.

Figure III.11 shows the frequency response of the white light source. In this figure it can be seen that the system has an approximately flat frequency response between 544.945 THz and 545.209 THz. This corresponds to wavelengths between 549.867nm and 550.133nm, which corresponds to green color.

To investigate the VLC channel response different amounts of noise are added to the signal in the over different add noise a time response has to compared before and after the VLC channel. Figure III.12, Figure III.13 and Figure III.14 show the time domain plot of the noise added to 10 symbols transmitted, where noise power was set to 0.5 W, 1W and 2W, respectively. Note the y axis was scaled differently in the figures.

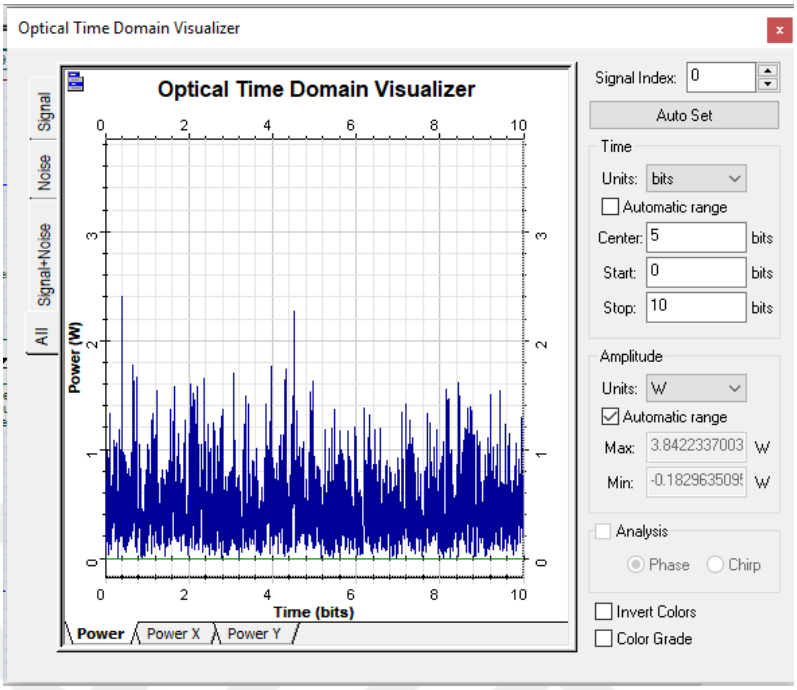

Figure III.12. Time response for 10 bits with 0.5W.

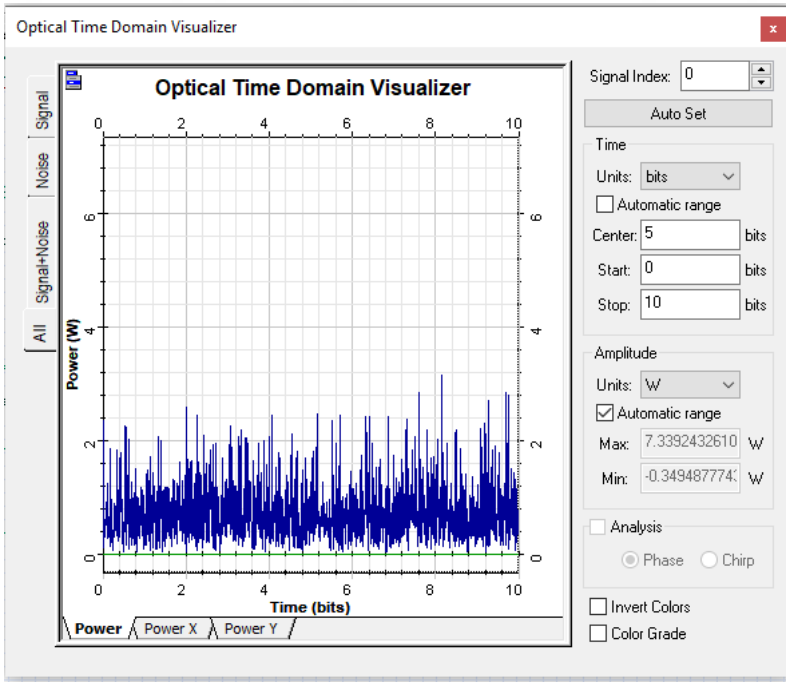

Figure III.13. Time response for 10 bits with 1W.

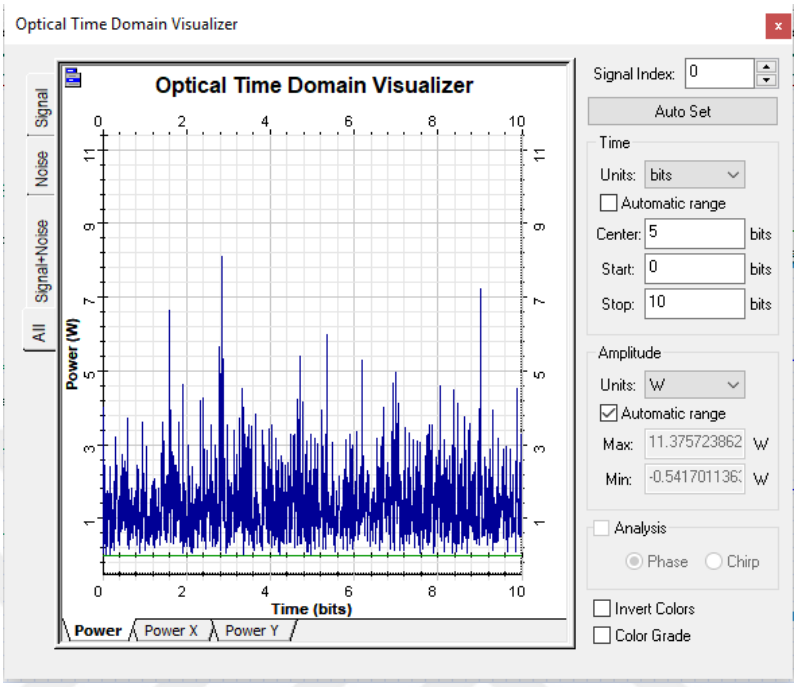

Figure III.14. Time response for 10 bits with 2W.

In a VLC system the time synchronization will need to be achieved through some algorithm. In the OptiSystem simulation, delay compensation is built into the system. The transmitted and received signals are shown in Figure III.15. To calculate the delay, a dual port oscilloscope were used to compare the original bits from PRBS generator (lower plot, red signal in Figure III.15) with signal after the ideal low pass filter (upper plot, blue signal in Figure III.15). The cutoff frequency of the ideal LPF is set to 0.75 of the sample rate.

It is seen that the effect of the LPF is to almost completely eliminate noise, however the shape of the pulses has been modified due to the Matlab channel and the LPF. There is significant inter-symbol interference created in this system.

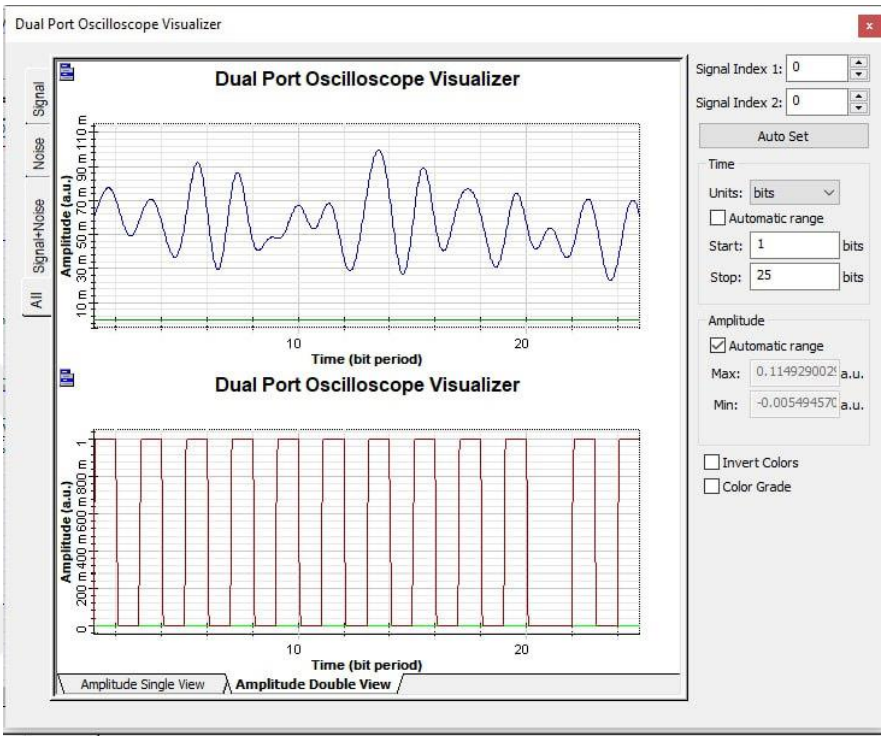

Figure III.15. Compare the original bits from PRBS generator (red signal) with signal after lowpass rectangular filter (blue signal).

3.6. Results

In this work the Q-factor, bit error rate and eye diagram were used for investigate the proposed VLC system performance. The data transmission rate, link distance and the average noise power is varied in simulations. The noise added corresponds to ambient light from both natural sources and other vehicles during communication.

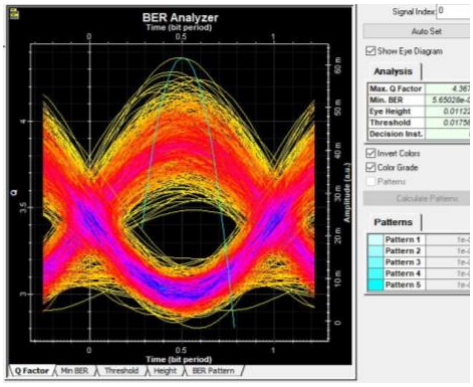

(a) Noise 0.5W, Bitrate 0.8 Gbps

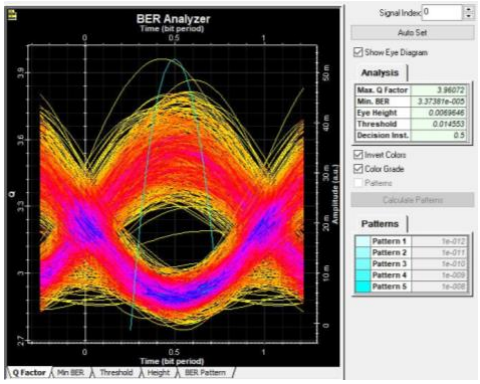

(b) Noise 0.5W, Bitrate 5 Gbps

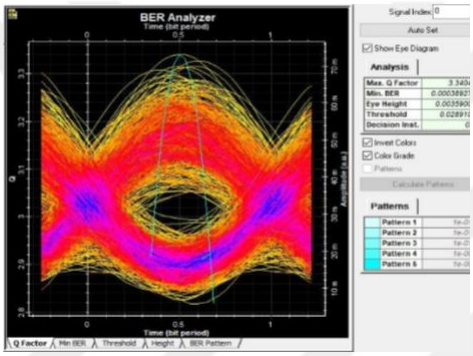

(c) Noise 1W, Bitrate 0.8 Gbps

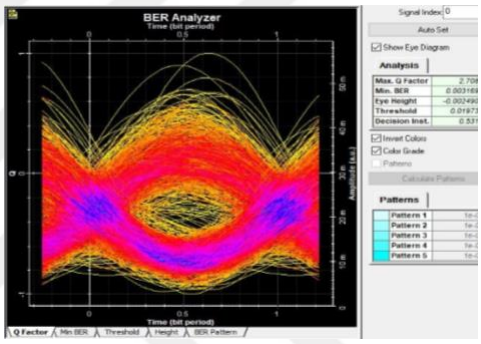

(d) Noise 1W, Bitrate 5 Gbps

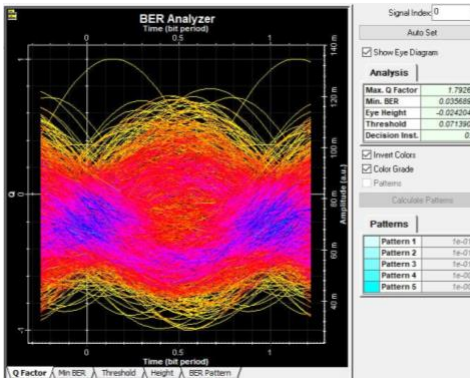

(e) Noise 3W, Bitrate 0.8 Gbps

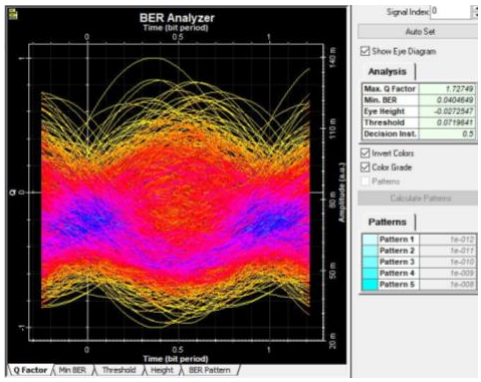

(f) Noise 3W, Bitrate 5 Gbps

Figure III.16. Eye diagrams of received signal at 1 meter distance.

Figure III.16 has six plots. These are plots of the eye diagram for the received signal at various noise magnitudes and transmission bit rates of 0.8Gbps and 4Gbps. It is clear from observing the eye diagrams that increasing bit rate and increasing ambient light noise will both degrade the signal and lead to bit errors.

Figure III.17 to Figure III.21 plot the Q-factor for the VLC receiver as the distance between transmitter and receiver is increased from 1 to 13 meters. Each figure shows the result for a different bit rate, from 0.8Gbps to 1.5Gbps. Each figure contains plots for six different levels of ambient light noise, from 0.2W to 3W. Figure III.22 to Figure III.26 show the BER under the same conditions.

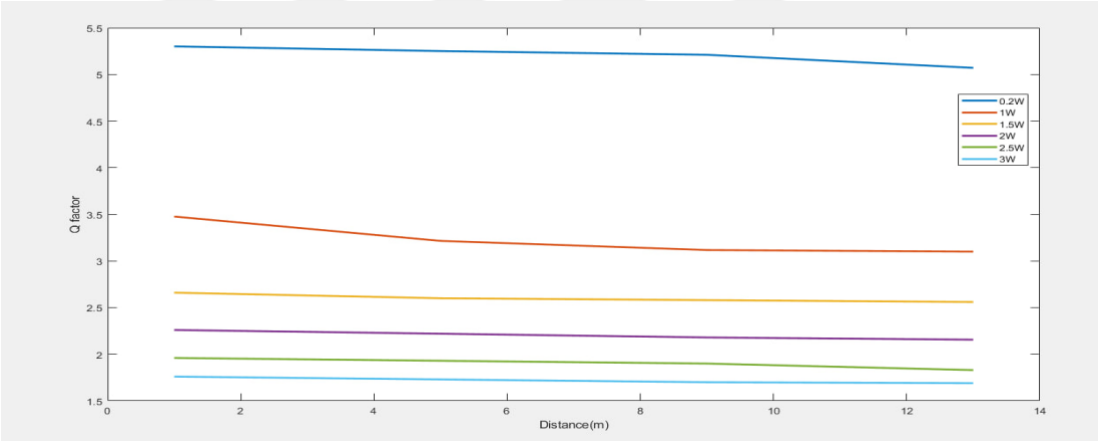

Figure III.17. Q factor values with distance at different external noise at data rate 0.8Gbps.

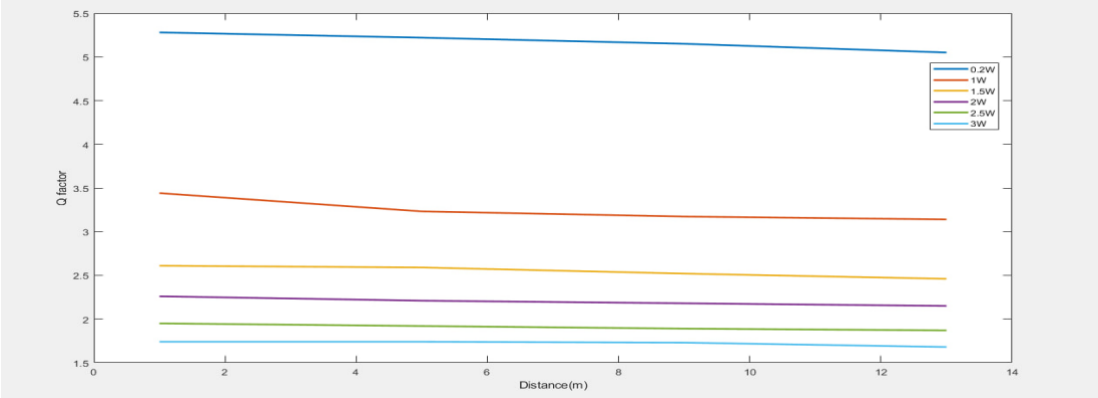

Figure III.18. Q factor values with distance at different external noise at data rate 0.9Gbps.

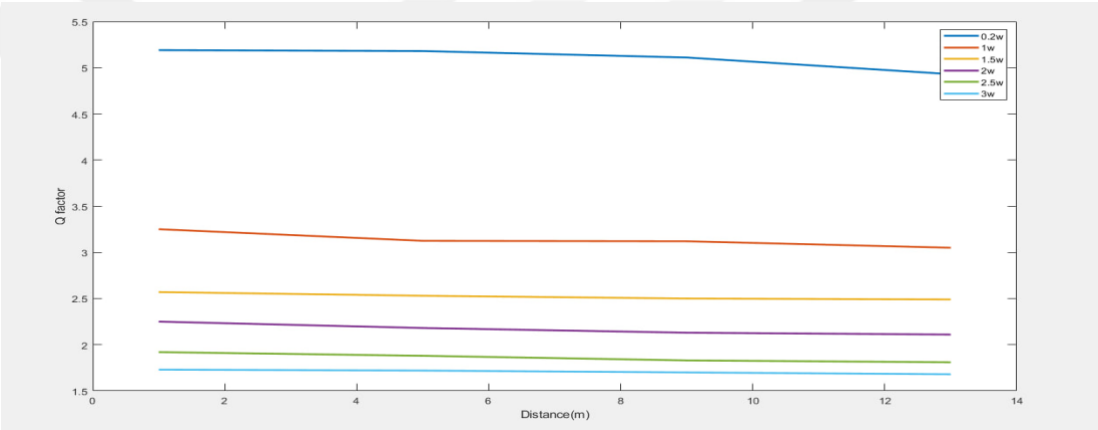

Figure III.19. Q factor values with distance at different external noise at data rate 1Gbps.

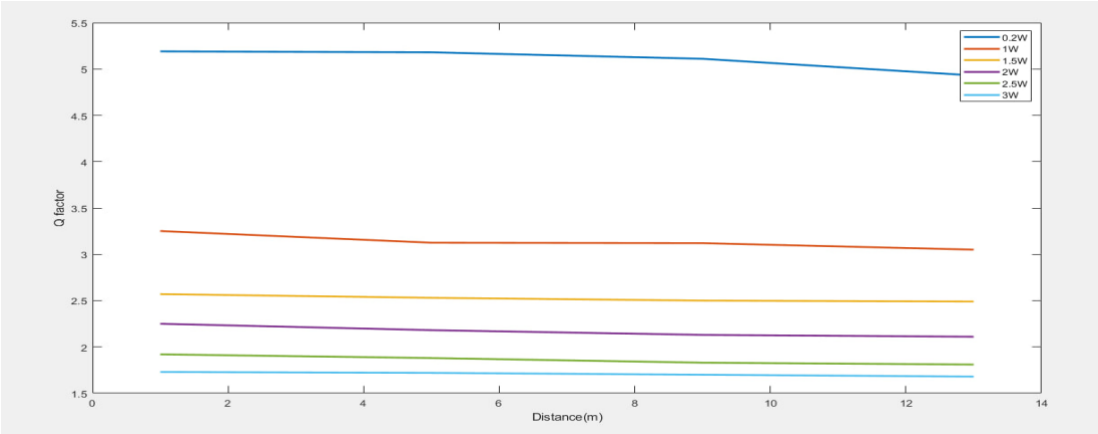

Figure III.20. Q factor values with distance at different external noise at data rate 1.2Gbps.

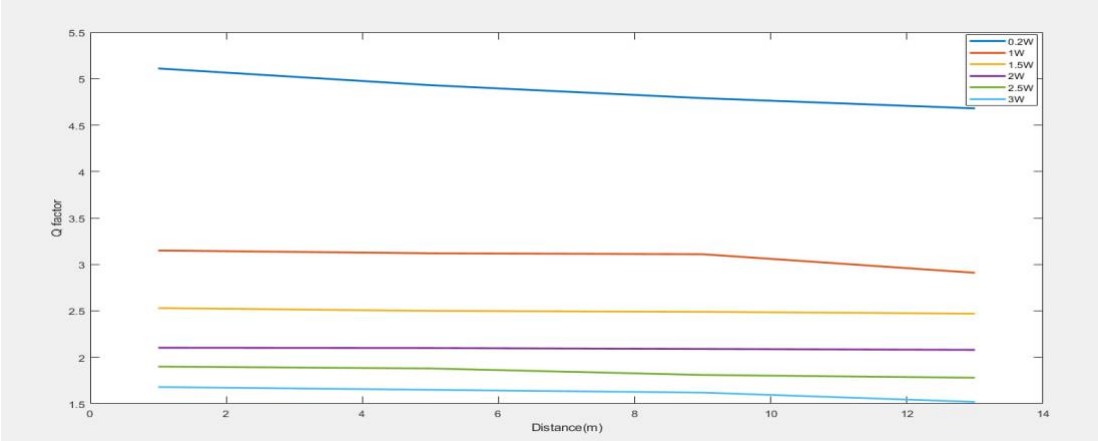

Figure III.21. Q factor values with distance at different external noise at data rate 1.5Gbps.

From these plots it can be seen that the Q factor decreases as the bit rate increases. Increasing link distance decreases received signal light intensity, but the difference of 12 meters does not in any case make up for a 0.5W increase in ambient light intensity. This means that the increase in light intensity and potentially the loss of line of sight signal due to the motion of the vehicles is much more important to the link reliability and link quality for VLC than the physical distance between the vehicles.

Figure III.22 to Figure III.26 are plots of the BER for the VLC receiver as the distance between transmitter and receiver is increased from 1 to 13 meters. Each figure shows the result for a different bit rate, from 0.8Gbps to 1.5Gbps. Each figure contains plots for six different levels of ambient light noise, from 0.2W to 3W. It is clear that increases in noise and distance of the link lead to higher bit error rate. The BER also increases when the rate of transmission increases, due to the inherent bandwidth of the channel.

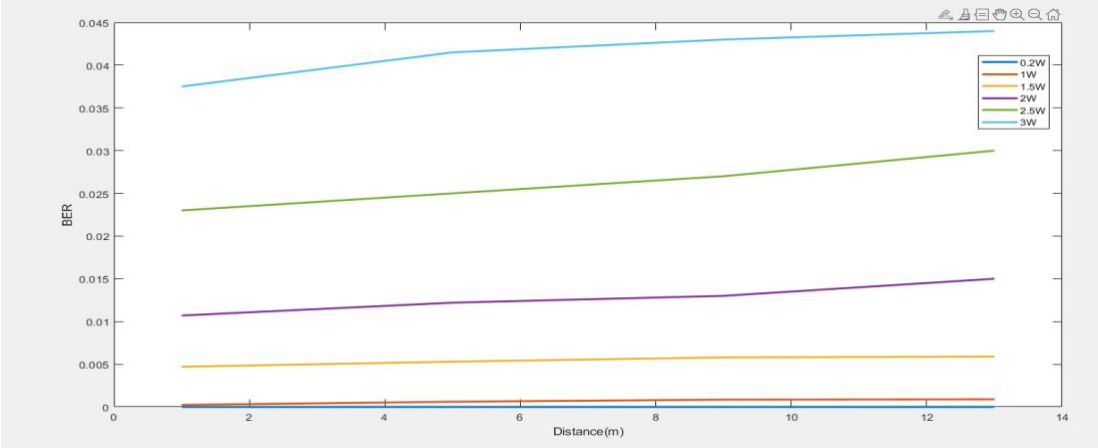

Figure III.22. BER across distance at different external noise at data rate 0.8 Gbps.

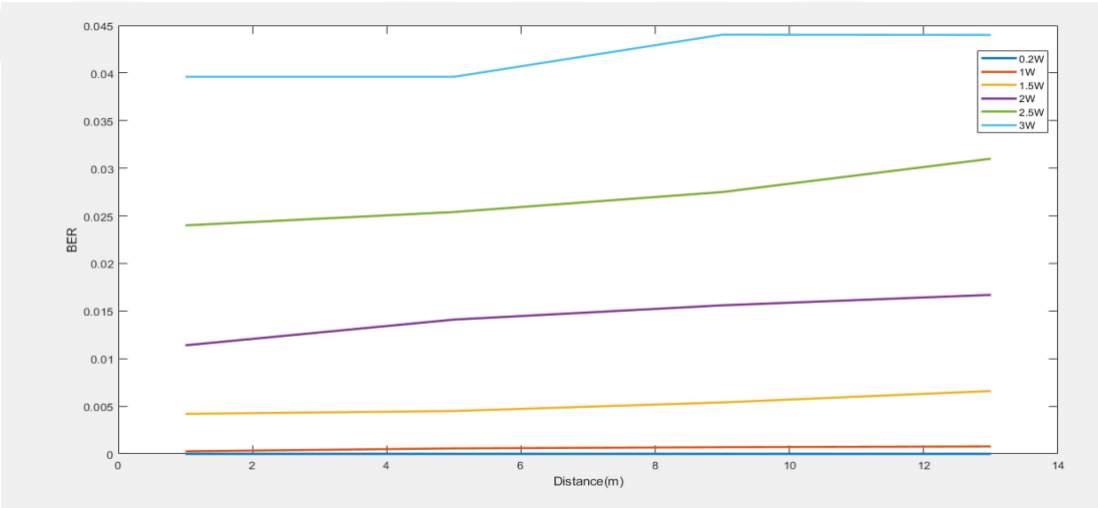

Figure III.23. BER across distance at different external noise at data rate 0.9 Gbps.

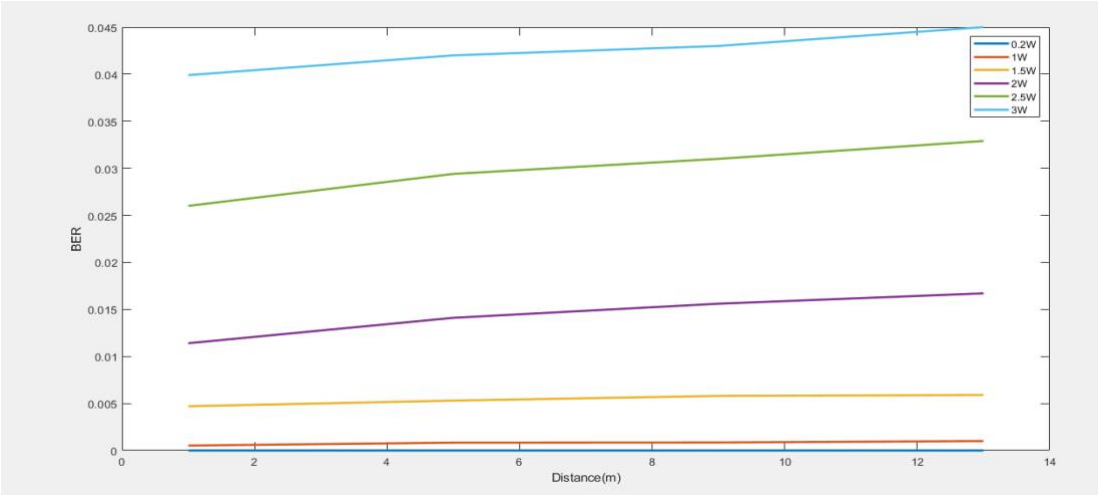

Figure III.24. BER across distance at different external noise at data rate 1 Gbps.

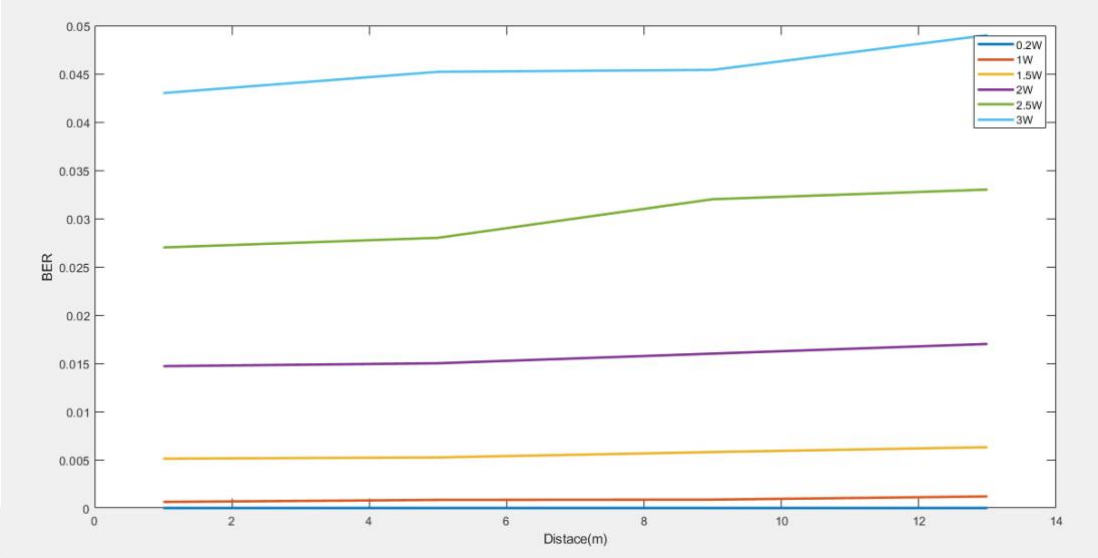

Figure III.25. BER across distance at different external noise at data rate 1.2 Gbps.

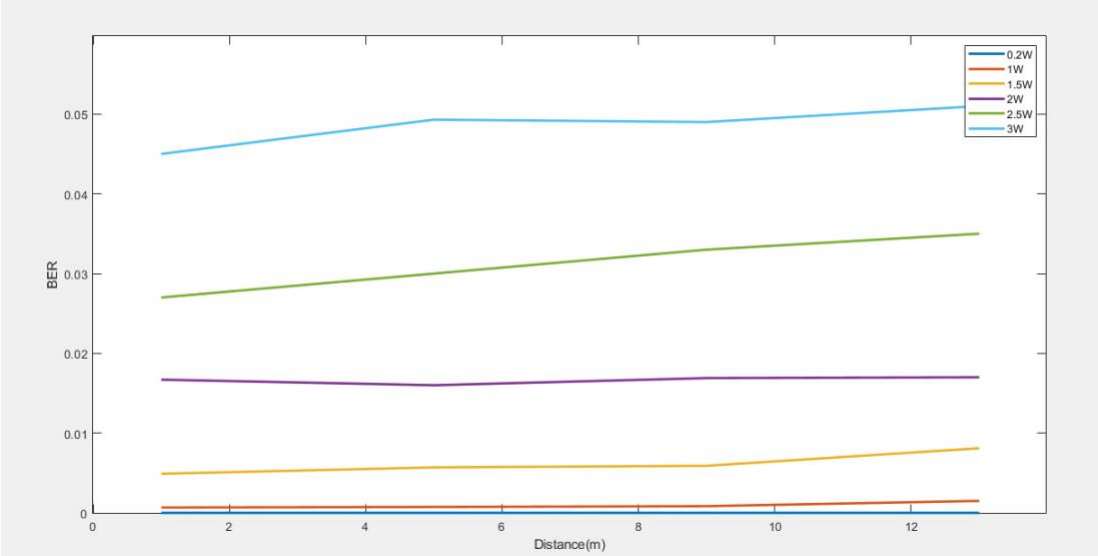

Figure III.26. BER across distance at different external noise at data rate 1.5 Gbps.

IV. SUMMARY AND CONCLUSIONS

This thesis has studied the performance of Visual Light Communication (VLC) for vehicular communication. Vehicular communication today inherently makes use of visual links, turn signals, caution lights and flashing of headlights allow drivers to communicate. It is possible to extend this technology to vehicle to vehicle and vehicle to infrastructure communications in order to provide high throughput reliable links for applications such as autonomous driving and accident prevention.

A search of the literature on VLC showed that VLC could provide a reliable mode of communication even across distances, in high ambient light and in adverse weather conditions such as snow and rain. This thesis described a model of an VLC communication system using green LED light. The model was generated on OptiSystem with a more detailed geometrically informed channel model implemented in Matlab. Simulation results showed that link quality and bit error rate depended on ambient light intensity, distance between transmitter and receiver and the transmitted symbol rate.

Weather conditions such as atmospheric turbulence, snow and rain were not considered in this study. Future work will focus on adding these effects. Another important point is interference and clutter noise due to communication between multiple vehicles on the road. Future work will also focus on adding this noise.

REFERENCES

[1] H. Elgala, “A Study on the Impact of Nonlinear Characteristics of LEDs on Optical OFDM,” Jacobs University, 2010.

[2] B. Mao, F. Tang, Y. Kawamoto, and N. Kato, “AI Models for Green Communications Towards 6G,” *IEEE Communications Surveys and Tutorials*, vol. 24, no. 1, pp. 210–247, 2022, doi: 10.1109/COMST.2021.3130901.

[3] Z. Wang, Q. Wang, W. Huang, and Z. Xu, *Visible Light Communications: Modulation and Signal Processing*. IEEE, 2017.

[4] Optisystem, “Optiwave,” 2022. https://optiwave.com/optisystem-overview/ (accessed May 10, 2023).

[5] A. Memedi and F. Dressler, “Vehicular visible light communications: A survey,” *IEEE Communications Surveys and Tutorials*, vol. 23, no. 1, pp. 161–181, 2021, doi: 10.1109/COMST.2020.3034224.

[6] M. Alsabah *et al.*, “6G Wireless Communications Networks: A Comprehensive Survey,” *IEEE Access*, vol. 9, pp. 148191–148243, 2021, doi: 10.1109/ACCESS.2021.3124812.

[7] Md. Noor-A-Rahim *et al.*, “6G for Vehicle-to-Everything (V2X) Communications: Enabling Technologies, Challenges, and Opportunities,” Dec. 2020.

[8] A. R. Ndjiongue and H. C. Ferreira, “An overview of outdoor visible light communications,” *Transactions on Emerging Telecommunications Technologies*, vol. 29, no. 7, pp. 1–15, 2018, doi: 10.1002/ett.3448.

[9] E. Zadobrischi and M. Damian, “Vehicular communications utility in road safety applications: A step toward self-aware intelligent traffic systems,” *Symmetry (Basel)*, vol. 13, no. 3, pp. 1–22, 2021, doi: 10.3390/sym13030438.

[10] B. Turan, G. Gurbilek, A. Uyrus, and S. C. Ergen, “Vehicular VLC Frequency Domain Channel Sounding and Characterization,” in *2018 IEEE Vehicular Networking Conference (VNC)*, IEEE, Dec. 2018, pp. 1–8. doi: 10.1109/VNC.2018.8628323.

[11] G. Gurbilek, M. Koca, B. Turan, and S. C. Ergen, “Poster: Vehicular VLC Experimental Modulation Performance Comparison,” *IEEE Vehicular Networking Conference, VNC*, vol. 2018-Decem, pp. 1–2, 2019, doi: 10.1109/VNC.2018.8628432.

[12] G. Gurbilek, M. Koca, and S. Coleri, “Blind channel estimation for DCO-OFDM based vehicular visible light communication,” *Physical Communication*, vol. 56, p. 101942, 2023, doi: 10.1016/j.phycom.2022.101942.

[13] B. Turan and S. Coleri, “Machine Learning Based Channel Modeling for Vehicular Visible Light Communication,” *IEEE Trans Veh Technol*, vol. 70, no. 10, pp. 9659–9672, 2021, doi: 10.1109/TVT.2021.3107835.

[14] M. S. Amjad *et al.*, “Towards an IEEE 802.11 Compliant System for Outdoor Vehicular Visible Light Communications,” *IEEE Trans Veh Technol*, vol. 70, no. 6, pp. 5749–5761, Jun. 2021, doi: 10.1109/TVT.2021.3075301.

[15] A. R. Ndjiongue, T. M. N. Ngatched, O. A. Dobre, and A. G. Armada, “VLC-Based Networking: Feasibility and Challenges,” *IEEE Netw*, vol. 34, no. 4, pp. 158–165, Jul. 2020, doi: 10.1109/MNET.001.1900428.

[16] S. Aboagye, A. R. Ndjiongue, T. M. N. Ngatched, O. A. Dobre, and H. V. Poor, "RIS-Assisted Visible Light Communication Systems: A Tutorial," *IEEE Communications Surveys & Tutorials*, vol. 25, no. 1, pp. 251–288, 2023, doi: 10.1109/COMST.2022.3225859.

[17] A. R. Ndjiongue, T. M. N. Ngatched, O. A. Dobre, and H. Haas, "Toward the Use of Re-configurable Intelligent Surfaces in VLC Systems: Beam Steering," *IEEE Wirel Commun*, vol. 28, no. 3, pp. 156–162, Jun. 2021, doi: 10.1109/MWC.001.2000365.

[18] R. C. Fon, A. R. Ndjiongue, and K. Ouahada, "Cascaded Optic Fibre–Visible Light Communications: Channel Model and Analysis," in *2019 International Conference on Advances in Big Data, Computing and Data Communication Systems (icABCD)*, IEEE, Aug. 2019, pp. 1–6. doi: 10.1109/ICABCD.2019.8851031.

[19] R. C. Fon, A. R. Ndjiongue, K. Ouahada, and A. M. Abu-Mahfouz, "Fibre optic-VLC versus laser-VLC: a review study," *Photonic Network Communications*, Jun. 2023, doi: 10.1007/s11107-023-00997-z.

[20] A. Al-Kinani, C.-X. Wang, L. Zhou, and W. Zhang, "Optical Wireless Communication Channel Measurements and Models," *IEEE Communications Surveys & Tutorials*, vol. 20, no. 3, pp. 1939–1962, 2018, doi: 10.1109/COMST.2018.2838096.

[21] F. M. Alsalami, Z. Ahmad, O. Haas, and S. Rajbhandari, "Regular-shaped geometry-based stochastic model for vehicle-to-vehicle visible light communication channel," *2019 IEEE Jordan International Joint Conference on*

Electrical Engineering and Information Technology, JEEIT 2019 - Proceedings, pp. 297–301, 2019, doi: 10.1109/JEEIT.2019.8717408.

[22] F. M. Alsalami, O. C. L. Haas, A. Al-Kinani, C.-X. Wang, Z. Ahmad, and S. Rajbhandari, "Impact of Dynamic Traffic on Vehicle-to-Vehicle Visible Light Communication Systems," *IEEE Syst J*, vol. 16, no. 3, pp. 3512–3521, Sep. 2022, doi: 10.1109/JSYST.2021.3100257.

[23] R. W. Zaki, H. A. Fayed, A. A. El Aziz, and M. H. Aly, "Outdoor visible light communication in intelligent transportation systems: Impact of snow and rain," *Applied Sciences (Switzerland)*, vol. 9, no. 24, 2019, doi: 10.3390/app9245453.

[24] S. A. Avătămăniței, A.-M. Căilean, A. Done, M. Dimian, and M. Prelipceanu, "Noise Resilient Outdoor Traffic Light Visible Light Communications System Based on Logarithmic Transimpedance Circuit: Experimental Demonstration of a 50 m Reliable Link in Direct Sun Exposure," *Sensors*, vol. 20, no. 3, p. 909, Feb. 2020, doi: 10.3390/s20030909.

[25] S.-A. Avatamanitei, A.-M. Cailean, A. Done, M. Dimian, and V. Popa, "Experimental Evaluation of Traffic Light to Vehicle Visible Light Communications in Snowfall Conditions," in *2020 7th International Conference on Control, Decision and Information Technologies (CoDIT)*, IEEE, Jun. 2020, pp. 693–696. doi: 10.1109/CoDIT49905.2020.9263837.

[26] S.-A. Avătămăniței, C. Beguni, A.-M. Căilean, M. Dimian, and V. Popa, "Evaluation of Misalignment Effect in Vehicle-to-Vehicle Visible Light Communications: Experimental Demonstration of a 75 Meters Link," *Sensors*, vol. 21, no. 11, p. 3577, May 2021, doi: 10.3390/s21113577.

[27] A.-M. Cailean, S.-A. Avatamanitei, C. Beguni, V. Popa, and M. Dimian, "Experimental Demonstration of a 188 meters Infrastructure-to-Vehicle Visible Light Communications Link in Outdoor Conditions," in *2021 IEEE Sensors Applications Symposium (SAS)*, IEEE, Aug. 2021, pp. 1–6. doi: 10.1109/SAS51076.2021.9530174.

[28] H. B. Eldeeb, M. Elamassie, S. M. Sait, and M. Uysal, "Infrastructure-to-Vehicle Visible Light Communications: Channel Modelling and Performance Analysis," *IEEE Trans Veh Technol*, vol. 71, no. 3, pp. 2240–2250, 2022, doi: 10.1109/TVT.2022.3142991.

[29] E. Eso, Z. Ghassemlooy, S. Zvanovec, J. Sathian, M. M. Abadi, and O. I. Younus, "Performance of vehicular visible light communications under the effects of atmospheric turbulence with aperture averaging," *Sensors*, vol. 21, no. 8, 2021, doi: 10.3390/s21082751.

[30] M. Huang, W. Guan, Z. Fan, Z. Chen, J. Li, and B. Chen, "Improved target signal source tracking and extraction method based on outdoor visible light communication using a cam-shift algorithm and Kalman filter," *Sensors (Switzerland)*, vol. 18, no. 12, 2018, doi: 10.3390/s18124173.

[31] R. Zhang, J. Wang, Z. Wang, Z. Xu, C. Zhao, and L. Hanzo, "Visible light communications in heterogeneous networks: Paving the way for user-centric design," *IEEE Wirel Commun*, vol. 22, no. 2, pp. 8–16, 2015, doi: 10.1109/MWC.2015.7096279.

[32] S. Fuada, A. P. Putra, Y. Aska, and T. Adiono, "Trans-impedance amplifier (HA) design for Visible Light Communication (VLC) using commercially available OP-AMP," in *2016 3rd International Conference on Information*

Technology, Computer, and Electrical Engineering (ICITACEE), IEEE, 2016, pp. 31–36. doi: 10.1109/ICITACEE.2016.7892405.

[33] Z. Ghassemlooy, L. N. Alves, S. Zvánovec, and M.-A. Khalighi, Eds., *Visible Light Communications: Theory and Applications*. Boca Raton: CRC Press, 2016. doi: 10.1201/9781315367330.

[34] R. Paschotta, "Gaussian Beams," *RP Photonics Encyclopedia*, 2023. https://www.rp-photonics.com/gaussian_beams.html (accessed Jan. 01, 2023).

[35] M. D. Soltani, A. A. Purwita, Z. Zeng, H. Haas, and M. Safari, "Modeling the random orientation of mobile devices: Measurement, analysis and LiFi Use Case," *IEEE Transactions on Communications*, vol. 67, no. 3, pp. 2157–2172, 2019, doi: 10.1109/TCOMM.2018.2882213.

[36] R. Hamagami, T. Ebihara, N. Wakatsuki, and K. Mizutani, "Optimal Modulation Technique for Underwater Visible Light Communication Using Rolling-Shutter Sensor," *IEEE Access*, vol. 9, pp. 146422–146436, 2021, doi: 10.1109/ACCESS.2021.3123358.

[37] T. Tang, T. Shang, and Q. Li, "Impact of Multiple Shadows on Visible Light Communication Channel," *IEEE Communications Letters*, vol. 25, no. 2, pp. 513–517, Feb. 2021, doi: 10.1109/LCOMM.2020.3031645.

[38] X. Yu, J. Wang, and H. Lu, "Single LED-Based Indoor Positioning System Using Multiple Photodetectors," *IEEE Photonics J*, vol. 10, no. 6, pp. 1–8, Dec. 2018, doi: 10.1109/JPHOT.2018.2848947.

[39] J. M. Senior and M. Y. Jamro, *Optical fiber communications: principles and practice*. Pearson, 2009.

[40] Z. Ghassemlooy, W. Popoola, and S. Rajbhandari, *Optical wireless communications: system and channel modelling with Matlab*. Second edition. | Boca Raton, FL : CRC Press/Taylor & Francis Group, 2018.: CRC Press, 2019. doi: 10.1201/9781315151724.

[41] S. Schmid, G. Corbellini, S. Mangold, and T. R. Gross, "LED-to-LED visible light communication networks," in *Proceedings of the fourteenth ACM international symposium on Mobile ad hoc networking and computing - MobiHoc '13*, New York, New York, USA: ACM Press, 2013, p. 1. doi: 10.1145/2491288.2491293.

[42] H. Zhao, G. Liu, J. Zhang, R. A. Arif, and N. Tansu, "Analysis of Internal Quantum Efficiency and Current Injection Efficiency in III-Nitride Light-Emitting Diodes," *Journal of Display Technology*, vol. 9, no. 4, pp. 212–225, Apr. 2013, doi: 10.1109/JDT.2013.2250252.

[43] J. Pfrommer, C. Zimmerling, J. Liu, L. Kärger, F. Henning, and J. Beyerer, "Optimisation of manufacturing process parameters using deep neural networks as surrogate models," *Procedia CIRP*, vol. 72, no. March, pp. 426–431, 2018, doi: 10.1016/j.procir.2018.03.046.

[44] J.-H. Cheng and S.-F. Liu, "A study of manufacturing strategies for LED lighting product design," in *2017 International Conference on Applied System Innovation (ICASI)*, IEEE, May 2017, pp. 1465–1101. doi: 10.1109/ICASI.2017.7988193.

[45] H. Elgala, R. Mesleh, and H. Haas, "Indoor optical wireless communication: potential and state-of-the-art," *IEEE Communications Magazine*, vol. 49, no. 9, pp. 56–62, Sep. 2011, doi: 10.1109/MCOM.2011.6011734.

[46] M. A. Umair, M. Meucci, and J. Catani, “Strong Noise Rejection in VLC Links under Realistic Conditions through a Real-Time SDR Front-End,” *Sensors*, vol. 23, no. 3, p. 1594, Feb. 2023, doi: 10.3390/s23031594.

[47] D. Karunatilaka, F. Zafar, V. Kalavally, and R. Parthiban, “LED Based Indoor Visible Light Communications: State of the Art,” *IEEE Communications Surveys & Tutorials*, vol. 17, no. 3, pp. 1649–1678, 2015, doi: 10.1109/COMST.2015.2417576.

[48] U. A. Korai, F. K. Shaikh, S. Kalwar, K. K. Soothar, B. Muneer, and A. Solangi, “Analyzing the Quality of Free Space Optical Signal in Fog: A Case Study of Pakistan,” *Wirel Pers Commun*, vol. 95, no. 2, pp. 569–579, 2017, doi: 10.1007/s11277-016-3910-8.

[49] F. K. Yam and Z. Hassan, “Innovative advances in LED technology,” *Microelectronics J*, vol. 36, no. 2, pp. 129–137, Feb. 2005, doi: 10.1016/j.mejo.2004.11.008.

[50] T. Komine and M. Nakagawa, “Fundamental analysis for visible-light communication system using LED lights,” *IEEE Transactions on Consumer Electronics*, vol. 50, no. 1, pp. 100–107, Feb. 2004, doi: 10.1109/TCE.2004.1277847.

[51] C. A. Balanis, *Antenna Theory, Analysis and Design, 3rd Ed.* 2005.

[52] G. R. Osche, *Optical detection theory for laser applications*. Wiley, 2002.

[53] Z. Chen, S. Yu, T. Wang, G. Wu, S. Wang, and W. Gu, “Channel correlation in aperture receiver diversity systems for free-space optical communication,” *Journal of Optics*, vol. 14, no. 12, p. 125710, Dec. 2012, doi: 10.1088/2040-8978/14/12/125710.

[54] B. E. A. Saleh and M. C. Teich, *Fundamentals of photonics*. Wiley, 2019.

[55] P. H. Pathak, X. Feng, P. Hu, and P. Mohapatra, "Visible Light Communication, Networking, and Sensing: A Survey, Potential and Challenges," *IEEE Communications Surveys & Tutorials*, vol. 17, no. 4, pp. 2047–2077, 2015, doi: 10.1109/COMST.2015.2476474.

[56] J. D. Gibson, *The communications handbook*. CRC press, 2018.

[57] Q. Wu and R. Zhang, "Towards Smart and Reconfigurable Environment: Intelligent Reflecting Surface Aided Wireless Network," *IEEE Communications Magazine*, vol. 58, no. 1, pp. 106–112, Jan. 2020, doi: 10.1109/MCOM.001.1900107.

[58] R. J. McIntyre, "Multiplication noise in uniform avalanche diodes," *IEEE Trans Electron Devices*, vol. ED-13, no. 1, pp. 164–168, Jan. 1966, doi: 10.1109/T-ED.1966.15651.

[59] J. B. Johnson, "Thermal agitation of electricity in conductors," *Physical Review*, vol. 32, no. 1, pp. 97–109, 1928, doi: 10.1103/PhysRev.32.97.

[60] J. I. Pankove, *Optical processes in semiconductors*. Courier Corporation, 1975.

[61] R. Loudon, *The quantum theory of light*. OUP Oxford, 2000.

[62] M. S. Keshner, "1/f noise," *Proceedings of the IEEE*, vol. 70, no. 3, pp. 212–218, 1982, doi: 10.1109/PROC.1982.12282.

[63] B. B. Adamczyk, K. Russa, and N. Hare, "Eye Diagram Part 1: Fundamental Concepts," *In Compliance*, no. August, pp. 48–51, 2022.

[64] A. Technologies, "Agilent 71501D Eye-Diagram Analysis User ' s Guide," 2002.

[65] Anritsu Company, "Understanding Eye Pattern Measurements," 2010.